Latent Mixture of Symmetries for Sample-Efficient Dynamic Learning

Haoran Li Chenhan Xiao Muhao Guo Yang Weng School of Electrical, Computer and Energy Engineering Arizona State University, Tempe, AZ 85281 {lhaoran, cxiao20, mguo26, yweng2}@asu.edu

Abstract

Learning dynamics is essential for model-based control and Reinforcement Learning in engineering systems, such as robotics and power systems. However, limited system measurements, such as those from low-resolution sensors, demand sampleefficient learning. Symmetry provides a powerful inductive bias by characterizing equivariant relations in system states to improve sample efficiency. While recent methods attempt to discover symmetries from data, they typically assume a single global symmetry group and treat symmetry discovery and dynamic learning as separate tasks, leading to limited expressiveness and error accumulation. In this paper, we propose the Latent Mixture of Symmetries (Latent MoS), an expressive model that captures a mixture of symmetry-governed latent factors from complex dynamical measurements. Latent MoS focuses on dynamic learning while locally and provably preserving the underlying symmetric transformations. To further capture long-term equivariance, we introduce a hierarchical architecture that stacks MoS blocks. Numerical experiments in diverse physical systems demonstrate that Latent MoS outperforms state-of-the-art baselines in interpolation and extrapolation tasks while offering interpretable latent representations suitable for future geometric and safety-critical analyses.

1 Introduction

Learning dynamic models is fundamental to modern physical and control systems, especially when exact governing equations are unavailable due to incomplete records, device aging, or privacy constraints [1, 2]. Accurate dynamic modeling enables robust control and Reinforcement Learning [3], and supports model-based analysis for performance and safety guarantees [4, 5]. However, sample-efficient learning remains a challenge in practice, where data scarcity arises from low-resolution meters, communication failures, or storage limitations. For example, in smart grids, SCADA (Supervisory Control and Data Acquisition) systems typically report measurements every $2 \sim 10$ seconds, while critical events may occur within milliseconds [6, 7].

To mitigate data scarcity issues, existing methods can be grouped into four main categories. The first category interpolates the low-resolution data by assuming sparsity [8], low-rankness [9], or manifold geometry [10]. The second category imposes known physical laws as constraints on the learning process [11, 12]. The third category utilizes Bayesian frameworks that demand accurate prior distributions [13–15]. In general, all of the above methods require certain domain-specific assumptions or knowledge. The fourth category requires little prior knowledge and leverages Ordinary Differential Equation (ODE) solvers to construct a continuous ODE process, e.g., the family of Neural ODEs [16–19]. Although Neural ODE-based methods are well-suited for sparse data, they often employ generic architectures such as multilayer perceptrons [16, 20]. This lack of inductive bias hinders generalization, leading to overfitting rather than capturing true dynamics.

To address these limitations, we propose to use the underlying symmetries in dynamical systems. Symmetry, defined as a group of transformations that leave a system's behavior or properties equivari-

ant [21], is prevalent across various domains. For instance, rotational, reflectional, and translational symmetries are leveraged in robotics [22], 3D vision data [23], power systems [24], fluid dynamics [25] and networked systems [26]. Why can symmetry increase sample efficiency? Intuitively, symmetry transformations enable a system state to represent a large set of equivariant states, reducing the amount of data needed for training. A rich line of work has shown the improvements of enforcing symmetry priors into equivariant neural networks [27–30] with some applications to sample-efficient RL [31–33]. Some other works investigate symmetry-based data augmentation [34] and regularization [35–37] for dynamic modeling. They rely on clear symmetry knowledge. For systems with unknown symmetries, several recent methods propose to discover symmetries from data [38–42].

However, these methods incur large modeling errors when applied to complex dynamical systems due to the following limitations: (1) *Decoupled learning and accumulated errors*. Symmetry discovery and dynamic modeling are typically treated as separate processes, leading to error propagation. (2) *Limited expressiveness of symmetry representations*. Most approaches assume that a single (linear or nonlinear) symmetry group governs at least a segment of data evolution. In practice, however, the underlying transformations exhibit substantial variability: both in *which* symmetries are relevant (often multi-modal and context-dependent), and in *when* they occur (ranging from short to long terms across distant segments). To summarize, dynamical systems often do not adhere to strict, rigid symmetry constraints, but instead exhibit forms of *symmetry breaking*. This means that while approximate symmetry structures are present, they may be only partially preserved or vary across regimes. Our work identifies symmetry breaking in two orthogonal axes: a mixture of groups and a short- or long-time dependence (see Section 2.1). The mixture of groups appears in literature [43], and the locally adaptable symmetry breaking is discussed in [44–46]. They are independently discussed, but our method addresses both in a unified framework.

To address these challenges, we introduce the following modeling strategies. First, grounded in Lie theory [47], we propose a dynamic learning model that preserves local symmetries in the latent space, thereby eliminating the need for symmetry discovery algorithms. Second, rather than relying on a single symmetry group, we consider a mixture of transformations inspired by the expressive mixture-based model [48]. We refer to the overall framework as the *Latent Mixture of Symmetries* (*Latent MoS*). Latent MoS encodes system evolution as a mixture of latent flows, each governed by a distinct Lie group. This design enables sample-efficient learning, as each flow captures a local symmetry transformation that defines a neighborhood of equivariant observations. Finally, to extend beyond local equivariance, we develop a hierarchical architecture by stacking multiple MoS blocks with different temporal resolutions. Namely, a higher level of MoS is responsible for modeling longer-term symmetries. In summary, our contributions are as follows:

- Latent MoS Framework: We propose the *Latent Mixture of Symmetries* (Latent MoS), a novel symmetry-preserving model that achieves high sample efficiency.
- **Theoretical Foundations**: We establish guarantees on the approximation capacity of Latent MoS and its ability to preserve symmetry structures induced by Lie group transformations.
- Empirical Validation: We demonstrate that Latent MoS outperforms state-of-the-art models across a variety of dynamical systems, particularly in low-resolution scenarios.

2 Preliminaries

Let $x \in \mathcal{X} \subseteq \mathbb{R}^n$ denote the system state. The discretized dynamics of the system are given by $x(t_{i+1}) = f(x(t_i))$, where $f: \mathcal{X} \to \mathcal{X}$ is an unknown dynamic function. The objective is to learn a model that approximates f using historical observations $\{x(t_i)\}_{i \in \mathcal{N}_x}$, which span the time interval from t_0 to t_N but can be low-resolution and irregularly sampled. For systems with inherent uncertainty, the goal becomes learning the transition probability distribution $p(x(t_{i+1}) \mid x(t_i))$. For notational simplicity, we focus on the deterministic setting and use f in the following derivations. In addition, the goal can also be extended to multi-horizon prediction, e.g., long-term forecasting.

2.1 Equivariance for Efficient Dynamic Learning

Intrinsic data scarcity challenges the learning process. Hence, we introduce the equivariance:

Definition 1. Let G be a symmetry group and a nonlinear group action be $\pi'_s(g,\cdot): G \times \mathcal{X} \to \mathcal{X}$. Then, the dynamic governing function f is G-equivariant if $\forall g \in G, x(t_i) \in \mathcal{X}$:

$$\pi'_s(g, \boldsymbol{x}(t_{i+1})) = f(\pi'_s(g, \boldsymbol{x}(t_i)). \tag{1}$$

When $\pi'_s(g,\cdot)$ is known or learned, existing methods use it to augment data [34] or impose symmetry constraints as regularization during training [37], thereby improving sample efficiency. While many recent models adopt this equivariance concept [32, 40, 37], we propose the following symmetry-breaking generalizations to suit more complex dynamical behaviors:

- **Temporal Dependence**. $\pi'_s(g,\cdot)$ may depend on time and past observations, requiring the learning model to be temporally adaptive. This extension is described in Section 3.2.
- Mixture of Groups: Multiple symmetry groups $\{G_1, \ldots, G_K\}$, such as the orthogonal group, the similarity group, the Euclidean group, and the affine group, may simultaneously influence the system dynamics. The mixture model is discussed in Section 3.2.
- Short- and Long-Term Equivariance: Symmetry relations may exist across multiple temporal scales. For example, $x(t_i)$ and $\pi'_s(g, x(t_i))$ may correspond to states that are either temporally close or far apart, depending on the choice of $g \in G$. However, traditional symmetry discovery methods often fail to capture long-term symmetries due to limited temporal modeling. Our approach to multi-scale symmetry is discussed in Section 3.3.

2.2 Nonlinear Group Action Decomposition

The nonlinear $\pi'_s(g,\cdot)$ is hard to analyze. [40] provides an effective decomposition for a compact Lie group G and a continuous group action $\pi'_s(g,\cdot)$ $(g \in G)$:

$$\pi'_s(g,\cdot) = f_{\text{dec}} \circ \pi_s(g) \circ f_{\text{enc}},$$
 (2)

where $f_{\text{enc}}: \mathcal{X} \to \mathcal{Z}$ and $f_{\text{dec}}: \mathcal{Z} \to \mathcal{X}$ are encoder and decoder neural networks between the state space \mathcal{X} and a latent space $\mathcal{Z} \subset \mathbb{R}^m$. $\pi_s: G \to \operatorname{GL}(m)$ is a group representation such that $\pi_s(g) \in \mathbb{R}^{m \times m}$ is a matrix that can transform a latent vector $z \in \mathcal{Z}$ by matrix multiplication. GL is the general linear group. Under mild assumptions, authors in [40] prove the *universal approximation* of a nonlinear group action using the decomposed format in Equation (2). Consequently, we only need to investigate the equivariant relation on \mathcal{Z} , which can be written as follows:

$$\forall g \in G, \mathbf{z}(t_i) \in \mathcal{Z}, \ \pi_s(g)\mathbf{z}(t_{i+1}) = f_z(\pi_s(g)\mathbf{z}(t_i)). \tag{3}$$

where $f_z = f_{\text{enc}} \circ f \circ f_{\text{dec}}$ is the dynamic function in \mathcal{Z} . It's easy to verify that when Equations (2) and (3) hold and the encoder and decoder are well-trained (i.e., $f_{\text{dec}} \circ f_{\text{enc}} = I$, where I is the identity matrix), the equivariant relation in Equation (1) also holds.

2.3 Time-Series Latent Space Construction

To construct the latent space for time-series measurements, we introduce Latent ODE [18] since it can explicitly model a continuous ODE process in \mathcal{Z} , capable of interpolating missing data at arbitrary times. In Latent ODE, ODE-RNN is the encoder (f_{enc}) to process $\{x(t_i)\}_{i\in\mathcal{N}_x}$ and generate a latent vector $z(t_0)$. The decoder (f_{dec}) employs a Neural ODE [16] to reconstruct the input state sequence and predict the future state. Mathematically, f_{enc} approximates the posterior:

$$q_{\phi}(z(t_0)|\{x(t_i)\}_{i\in\mathcal{N}_x}) = \mathcal{N}(\mu_0, \Sigma_0), \ \mu_0, \Sigma_0 = f_{\text{enc}}(\{x(t_i)\}_{i\in\mathcal{N}_x}), \tag{4}$$

where ϕ is the parameter set for f_{enc} that approximates the mean and the variance of the posterior $q_{\phi}(\boldsymbol{z}(t_0)|\{\boldsymbol{x}(t_i)\}_{i\in\mathcal{N}_x})$. The encoding process is shown on the bottom left of Fig. 1. The decoder uses $\boldsymbol{z}(t_0)$ as the initial latent state and solves the ODE problem for inference:

$$z(t_0) \sim p(z(t_0)), \ z(t_i) = \text{ODESolve}(h_\theta, z(t_0), t_i), \ x(t_i) \sim p_\theta(x(t_i)|z(t_i)),$$
 (5)

where θ is the parameter set for f_{dec} , $p(\boldsymbol{z}(t_0))$ is a zero-mean Gaussian, $h: \mathcal{Z} \to \mathcal{Z}$ is a neural network to represent the derivative $\dot{\boldsymbol{z}}(t)$, and p_{θ} includes several MLP layers to approximate the conditional distribution. Thus, f_{dec} consists of both h_{θ} and p_{θ} . The overall training maximizes the evidence lower bound (ELBO): $\text{ELBO}(\phi,\theta) = \mathbb{E}_{\boldsymbol{z}(t_0) \sim q_{\phi}} \log p_{\theta}(\{\boldsymbol{x}(t_i)\}_{i \in \mathcal{N}_x})) - \text{KL}\left[q_{\phi}(\boldsymbol{z}(t_0)|\{\boldsymbol{x}(t_i)\}_{i \in \mathcal{N}_x})||p(\boldsymbol{z}(t_0))\right]$. For the deterministic scenario, we can also minimize the Mean Square Error (MSE). The bottom right of Fig. 1 shows the decoding process.

3 Method

In this section, we introduce a dynamic learning model that intrinsically preserves complex symmetries (Section 2.1) without symmetry discovery. By embedding geometric priors into the latent dynamics in Equation (3), we enforce physically grounded, symmetry-preserving structure with theoretical guarantees (Section 3.1). This foundation extends to a mixture model (Section 3.2) and generalizes to multi-scale temporal equivariance (Section 3.3).

3.1 Short-term Equivariance Preservation for A Single Latent Symmetry

We begin with the ideal case where the dynamics are governed by symmetry transformations of a single Lie group G. Then, we examine the functional class of dynamic models that have the potential to preserve equivariance. An expressive class is the dynamic function that can *commute with* the transformation in G. For example, the rotating dynamics in a 2D circle can commute with the rotational action in SO(2), and thus are SO(2)-equivariant. SO is the special orthogonal group. In general, to study the commutative property, we demand the dynamic itself to be a Lie group action. Specifically, we consider the nonlinear Lie group action $\pi'_d(h,\cdot)$ such that:

$$\pi'_d(h,\cdot) = f_{\text{dec}} \circ \pi_d(h) \circ f_{\text{enc}}, \ \ z(t_{i+1}) = f_z(z(t_i)) := \pi_d(h)z(t_i),$$
 (6)

where we use the subscript d to respect the dynamics. $h \in H$ and H is another Lie group that represents dynamics. By the universal approximation in Section 2.2, $\pi'_d(h, \cdot)$ can be decomposed, as shown in the first equality in Equation (6). Thus, we only need to focus on the property of the matrix transformation $\pi_d(h)$ operating in \mathcal{Z} . The following lemma illustrates how $\pi_d(h)$ can commute with $\pi_s(g)$ to preserve the equivariance.

Lemma 1. Assume that G and $H \subseteq G$ are Lie groups whose elements are defined in Equation (6) and Equation (3), respectively. Define the centralizer of H in G as: $C_G(h) := \{g \in G | \pi_s(g)\pi_d(h) = \pi_d(h)\pi_s(g)\}$. If $C_G(h)$ is nontrivial (i.e., contains elements other than the identity), then $\forall g \in C_G(h)$, the relation for $\pi_s(g)$ in Equation (3) is preserved.

The proof is in Appendix A.1. The commutative property in the centralizer $C_G(h)$ defines an equivalent format for G-equivariance. In Lemma 1, the first condition $(h \in H \subseteq G)$ is ideal by assuming a globally constant dynamic function and a single Lie group G. Hence, in Section 3.2, we design the learning model capable of capturing mixed and time-variant symmetries. The second condition $(C_G(h))$ is nontrivial) doesn't always hold. Thus, we establish the following conditions.

Proposition 1 (Sufficient Conditions for Nontrivial Centralizer). Let $H \subset Aff(m)$ be an affine Lie subgroup whose elements are represented in homogeneous coordinates as affine transformations:

$$\pi_d(h)\tilde{\boldsymbol{z}}(t) := \begin{bmatrix} A_h & \boldsymbol{b}_h \\ \mathbf{0} & 1 \end{bmatrix} \begin{bmatrix} \boldsymbol{z}(t) \\ 1 \end{bmatrix}, \tag{7}$$

where $A_h \in GL(m)$, $\mathbf{b}_h \in \mathbb{R}^m$, and we use $\tilde{\mathbf{z}}(t) = [\mathbf{z}(t), 1]^{\top} \in \mathbb{R}^{m+1}$ to denote the augmented latent vector in homogeneous coordinates to support affine transformations. Suppose that for $\forall g, h \in H$, it holds that $A_g A_h = A_h A_g$, $A_g \mathbf{b}_h = \mathbf{b}_h$ and $A_h \mathbf{b}_g = \mathbf{b}_g$. Then we have $H \subseteq C_G(h)$. In particular, $C_G(h)$ is nontrivial and contains at least all of elements in H.

The proof is provided in Appendix A.2. In Equation (7), we adopt the upper-triangular affine matrix form because it offers a unified and compact representation for a broad class of Lie transformations, including *rotation*, *scaling*, and *translation*, and their higher-order multiplications. Subsequently, we show in Corollaries 1–3 that they satisfy the commutativity conditions in Proposition 1, thus having equivariance guarantees.

Corollary 1 (Equivariance of Planar Rotation Transformation). Let u_1 and u_2 be orthonormal vectors and $P := [u_1 \ u_2] \in \mathbb{R}^{m \times 2}$. Consider the planar rotation transformation: $\hat{\pi}^{rot} = \begin{bmatrix} I_m + P(R_{\theta} - I_2)P^{\top} & 0 \\ 0 & 1 \end{bmatrix}$, where $R_{\theta} = \begin{bmatrix} \cos \theta & -\sin \theta \\ \sin \theta & \cos \theta \end{bmatrix} \in SO(2)$, I_m is the $m \times m$ identify matrix. Then $\hat{\pi}^{rot}$ and its Lie subgroup $H \in SO(m)$ satisfy the conditions in Proposition 1.

The restriction to planar rotation arises because general rotations are non-commutative. E.g., a die rotates along the x-axis and then z-axis, or along the z-axis and then x-axis, will cause different results. In contrast, planar rotations (fixed rotation axis) are commutative. The result is rigorously proved in Appendix A.3, meaning that the state should rotate along one axis at least locally to preserve rotation symmetry. If a rotation continuously changes the axis, symmetry is completely removed. Although R_{θ} is two-dimensional, the learnable projection matrix can lift the dimension to increase the expressiveness of $\hat{\pi}^{rot}$.

Corollary 2 (Equivariance of Translation and Scaling Transformation). Denote the translation dynamics: $\hat{\pi}^{tra} = \begin{bmatrix} I_m & v \\ 0 & 1 \end{bmatrix}$ and its Lie subgroup $H \subset E(m)$, where E(m) is an Euclidean group.

They satisfy the conditions in Proposition 1. Denote the scaling dynamics:
$$\hat{\pi}^{sca} = \begin{bmatrix} \operatorname{diag}(\boldsymbol{\gamma}) & \mathbf{0} \\ \mathbf{0} & 1 \end{bmatrix}$$

and its Lie subgroup $H \subset Sim(m)$, where Sim(m) is a similarity group. They satisfy the conditions in Proposition 1.

Corollary 3 (Equivariance of Second-Order Composed Transformations). The second-order composition of the planar rotation, translation, and scaling transformations defined in Corollaries 1–2 satisfies the commutativity conditions in Proposition 1. Specifically, for any $\hat{\pi}^{(1)}$, $\hat{\pi}^{(2)} \in \{\hat{\pi}^{rot}, \hat{\pi}^{tra}, \hat{\pi}^{sca}\}$, we have that $\hat{\pi}^{(1)}\hat{\pi}^{(2)}$ and its Lie subgroup $H \subset \text{Aff}(m)$ satisfy the conditions in Proposition 1.

In corollary 1 to 3, we add $\hat{\cdot}$ to the matrix transformation to imply that it's a candidate dynamic approximation as we don't know the ground truth. The proof is provided in the Appendix A.3 to A.5.

3.2 Latent Mixture of Symmetries with Preserved Equivariance

Proposition 1 identifies a rich set of Lie groups that may appear in complex systems. In this section, we introduce our model to capture the mixture of diverse symmetries and maintain high representational power. Fig. 1 demonstrates the main architecture. The core is a Mixture-of-Experts (MoE) model, which employs a gating mechanism [49] to automatically select the appropriate Lie group transformations. In addition, we make the MoS module time-variant for time-dependent symmetries. Thanks to the model's extensibility, new Lie group experts that are not characterized by Proposition 1 can be flexibly incorporated. We leave such extensions for future work. Specifically, let $h \in \mathbb{R}^K$ be the output of a gating neural network, activated by a Softmax function. Treating each symmetry transformation as an expert, the k^{th} entry h[k] provides the weight for the expert. Then, Latent MoS linearly mixes the latent flows $\tilde{\boldsymbol{z}}_k(t_{i+1})$ such that:

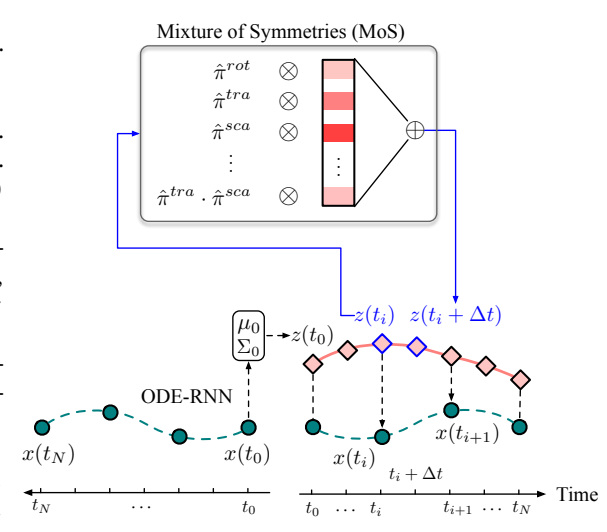


Figure 1: The Latent MoS framework. Compared to Latent ODE, Latent MoS *structures* the latent dynamics by using an MoE to select symmetries. Different colors in the MoS box imply different gate weights.

$$\tilde{z}(t_{i+1}) = \sum_{k=1}^{K} h[k] \cdot \tilde{z}_k(t_{i+1}) := \sum_{k=1}^{K} h[k] \cdot \hat{\pi}_k \cdot \tilde{z}(t_i), \tag{8}$$

where $\hat{\pi}_k$ is the k^{th} expert, parameterized to represent a Lie group action with a geometric structure from Proposition 1. We adopt a linear mixture because real-world systems often exhibit multiple latent symmetry flows acting simultaneously (e.g., damping and oscillation), which cannot be represented by a single Lie group action. The linear mix allows the gating network to combine these expert transformations into expressive latent dynamics, while still preserving the interpretability of each individual symmetry component.

In Equation (8), h and $\hat{\pi}_k$ are made of time-dependent. Specifically, let the time interval $[t_0, t_N]$ be evenly divided into L disjoint subintervals:

$$[t_0, t_N] = \bigcup_{l=0}^{L-1} [t^{(l)}, t^{(l+1)}), \quad \text{where} \quad t^{(l)} := t_0 + l \cdot \Delta T, \ \Delta T = \frac{t_N - t_0}{L}. \tag{9}$$

Then, for each subinterval, $\hat{\pi}_k$ and h are piecewise constant and locally dependent on both the initial time $t^{(l)}$ and the latent state $\tilde{z}(t^{(l)})$, i.e., $h := h(t^{(l)}, z(t^{(l)}))$ and $\hat{\pi}_k := \hat{\pi}_k(t^{(l)}, z(t^{(l)}))$. The specific designs for $\hat{\pi}_k$ are shown below. We eliminate the superscript (l) for simplicity.

Rotational symmetry. The group action $\hat{\pi}^{rot}(t, \boldsymbol{z}(t)) \in \operatorname{SE}(m)$, where $\operatorname{SE}(m)$ is a special Euclidean group. To parameterize $\hat{\pi}^{rot}(t, \boldsymbol{z}(t))$, by Corollary 1, we first learn a projection matrix $\hat{P}(t, \boldsymbol{z}(t)) \in \mathbb{R}^{m \times 2}$, whose columns form an orthonormal basis of a 2D subspace in \mathbb{R}^m . Specifically, a neural network outputs an unconstrained matrix $\hat{V}(t, \boldsymbol{z}(t)) \in \mathbb{R}^{m \times 2}$, which is then orthonormalized via a QR decomposition: $\hat{V}(t, \boldsymbol{z}(t)) = \hat{Q}(t, \boldsymbol{z}(t))\hat{R}(t, \boldsymbol{z}(t))$, and we define $\hat{P}(t, \boldsymbol{z}(t)) := \hat{Q}(t, \boldsymbol{z}(t))$. We also parameterize a planar rotation matrix $R_{\theta} \in \operatorname{SO}(2)$ using a learnable scalar angle $\theta(t, \boldsymbol{z}(t))$. The

overall transformation is then defined as: $\hat{\pi}^{rot}(t, \boldsymbol{z}(t)) := \begin{bmatrix} I_m + \hat{P}(R_{\theta} - I_2)\hat{P}^{\top} & \mathbf{0} \\ \mathbf{0}^{\top} & 1 \end{bmatrix} \in SE(m)$, which applies a learned planar rotation within a dynamically selected 2D subspace while leaving the rest of the space invariant and preserving the affine structure.

Translational symmetry. The action $\hat{\pi}^{tra}(t, \boldsymbol{z}(t)) \in E(m)$, where E(m) is an Euclidean group. Given a learnable velocity vector $\boldsymbol{v}(t, \boldsymbol{z}(t)) \in \mathbb{R}^m$, we define: $\hat{\pi}^{tra}(t, \boldsymbol{z}(t)) = \begin{bmatrix} I & \boldsymbol{v}(t, \boldsymbol{z}(t)) \\ \boldsymbol{0} & 1 \end{bmatrix}$.

Scaling symmetry. The group action $\hat{\pi}^{sca}(t, \boldsymbol{z}(t)) \in \operatorname{Sim}(m)$, where $\operatorname{Sim}(m)$ is a similarity group. For a ratio vector $\boldsymbol{\gamma}(t, \boldsymbol{z}(t)) \in \mathbb{R}^m$, we have $\hat{\pi}^{sca}(t, \boldsymbol{z}(t)) = \begin{bmatrix} \operatorname{diag}(\boldsymbol{\gamma}(t, \boldsymbol{z}(t))) & \mathbf{0} \\ \mathbf{0} & 1 \end{bmatrix}$.

Second-order multiplications. To capture coupled symmetry effects, we consider the multiplication of multiple Lie group actions. For example, multiplying a translational action $\hat{\pi}^{tra}(t, \boldsymbol{z}(t))$ with a scaling action $\hat{\pi}^{sca}(t, \boldsymbol{z}(t))$ yields a new transformation $\hat{\pi}^{com}(t, \boldsymbol{z}(t)) = \hat{\pi}^{tra}(t, \boldsymbol{z}(t)) \cdot \hat{\pi}^{sca}(t, \boldsymbol{z}(t))$. More generally, the multiplication of Lie group actions remains a valid Lie group action when defined over a closed subgroup (e.g., SE(m), E(m), Sim(m), etc.).

Fig. 1 illustrates how the gating mechanism enables a mixture of symmetry transformations to govern the latent dynamics. Compared to the Latent ODE model introduced in Section 2.3, our Latent Mixture of Symmetries (Latent MoS) replaces the unstructured ODE update step (i.e., ODESolve in Equation (5)) with a structured, symmetry-preserving formulation as given in Equation (8). According to Proposition 1, each latent flow $\tilde{z}_k(t)$ in Equation (8) preserves an underlying equivariance, which facilitates more sample-efficient learning.

Discrete vs. continuous updates. Equation (8) adopts a discrete update formulation based on Lie group actions. However, our framework also admits a continuous-time integral by computing the matrix logarithm of the group action to obtain its infinitesimal generator. Specifically, for each expert, we define $\hat{\xi}_k(t, \boldsymbol{z}(t)) := \log\left(\hat{\pi}_k(t, \boldsymbol{z}(t))\right)$, where $\hat{\xi}_k \in \mathfrak{g}$ is the Lie algebra element corresponding to $\hat{\pi}_k \in G$. This enables continuous integration of the latent trajectory via the Lie algebra. Specifically, for the k^{th} flow, the evolution of $\tilde{\boldsymbol{z}}(t)$ is governed by the differential equation $\frac{d}{dt}\tilde{\boldsymbol{z}}_k(t) = \hat{\xi}_k(t, \boldsymbol{z}(t)) \cdot \tilde{\boldsymbol{z}}(t)$, whose solution over a small interval $[t_i, t_i + \Delta t]$ is given by the matrix integral: $\tilde{\boldsymbol{z}}_k(t_i + \Delta t) = \exp\left(\int_{t_i}^{t_i + \Delta t} \hat{\xi}_k(s, \boldsymbol{z}(s)) \, ds\right) \cdot \tilde{\boldsymbol{z}}(t_i)$. While this formulation enables interpolation and handling of irregular time intervals, computing the integral and exponential map can be computationally expensive. By the first-order approximation of Lie group flows [50], we can approximate the matrix integral as $\tilde{\boldsymbol{z}}_k(t_i + \Delta t) \approx \exp\left(\Delta t \cdot \hat{\boldsymbol{\xi}}_k(t_i, \boldsymbol{z}(t_i))\right) \cdot \tilde{\boldsymbol{z}}(t_i)$. With a slight abuse of notation, we then define the group action $\hat{\pi}_k(t^{(i)}, \boldsymbol{z}(t^{(i)})) := \exp\left(\Delta t \cdot \hat{\boldsymbol{\xi}}_k(t^{(i)}, \boldsymbol{z}(t^{(i)}))\right)$, where $t_i \in [t^{(i)}, t^{(i+1)})$. This leads to the the discrete Δt update:

$$\tilde{z}(t_i + \Delta t) := \sum_{k=1}^{K} h(t^{(i)}, z(t^{(i)}))[k] \cdot \hat{\pi}_k(t^{(i)}, z(t^{(i)})) \cdot \tilde{z}(t_i).$$
(10)

Combing this equation with the Equation (8), we can obtain a high-resolution latent sequence $\tilde{z}_{0:N}(\Delta t) = (\tilde{z}(t_0), \tilde{z}(t_0 + \Delta t), \tilde{z}(t_0 + 2\Delta t), \cdots, \tilde{z}(t_N - \Delta t), \tilde{z}(t_N))$, which can be treated as features for interpolation and extrapolation, as shown in Equation (5). The bottom right part of Fig. 1 demonstrates the process: the green observations are sparse, but the pink latent vectors are dense.

3.3 Multi-scale Latent MoS for Short- and Long-term Equivariance

The transformation $\hat{\pi}_k(t^{(i)}, \boldsymbol{z}(t^{(i)}))$, defined only within the local interval $[t^{(l)}, t^{(l+1)})$, may fail to capture long-term equivariant relations. Specifically, there may exist a symmetry transformation $\pi_s(g)$ that maps $\boldsymbol{z}(t_i)$ to a point outside the current interval to preserve the dynamics, but it will be missed by locally defined models. To address this, we propose a simple hierarchical structure. Intuitively, we consider different durations for a constant dynamic function, illustrated in Algorithm 1. $L^i > L^j$ if level j corresponds to a higher and coarser resolution level.

Algorithm 1 Multi-level Latent Sequence Generation

```
 \begin{aligned} & \text{Require: Initial full latent state } \tilde{\boldsymbol{z}}(t_0) \in \mathbb{R}^m \text{, time step } \Delta t \text{, number of subintervals at different levels } \\ & \{L^{(1)}, L^{(2)}, \dots, L^{(S)}\}. \\ & \text{1: Partition } \tilde{\boldsymbol{z}}(t_0) \text{ into } [\tilde{\boldsymbol{z}}^{(1)}(t_0), \dots, \tilde{\boldsymbol{z}}^{(S)}(t_0)] \text{, where each } \tilde{\boldsymbol{z}}^{(s)}(t_0) \in \mathbb{R}^{m/S}. \\ & \text{2: for each level } s = 1 \text{ to } S \text{ do} \\ & \text{3: } \quad \text{Set } L \leftarrow L^{(s)}. \text{ Use Equation (9) to compute the subintervals } \{[t^{(l)}, t^{(l+1)})\}_{l=0}^{L-1} \\ & \text{4: } \quad \text{for each subinterval } [t^{(l)}, t^{(l+1)}) \text{ do.} \\ & \text{5: } \quad \text{Generate MoS}^{(s)} \colon \{\hat{\pi}_k(t^{(l)}, \tilde{\boldsymbol{z}}^{(s)}(t^{(l)}))\}_{k=1}^K \text{ and gates } h^{(s)}(t^{(l)}, \tilde{\boldsymbol{z}}^{(s)}(t^{(l)})). \\ & \text{6: } \quad \text{end for} \\ & \text{7: } \quad \text{Use Equation (10) to gain a trajectory } \tilde{\boldsymbol{z}}_{0:N}^{(s)}(\Delta t) = \left(\tilde{\boldsymbol{z}}^{(s)}(t_0), \tilde{\boldsymbol{z}}^{(s)}(t_0 + \Delta t), \dots, \tilde{\boldsymbol{z}}^{(s)}(t_N)\right). \\ & \text{8: end for} \\ & \text{9: } \quad \text{return } \tilde{\boldsymbol{z}}_{0:N}(\Delta t) = \text{concat } \left(\tilde{\boldsymbol{z}}_{0:N}^{(1)}(\Delta t), \dots, \tilde{\boldsymbol{z}}_{0:N}^{(S)}(\Delta t)\right) \text{ along the feature dimension.} \end{aligned}
```

4 Experiments

We test the following datasets, fully described in Appendix B. (1) Complex Nonlinear ODE **Systems.** Similar to [37], we employ spiral datasets, Glycolytic oscillators (biochemical system), and Lotka-Volterra systems (the interaction between a predator and a prey population). (2) **Residential Electricity Consumption.** We gather real-world electricity data, publicly available at [51–53]. (3) Photovoltaic Solar Energy. We introduce a publicly available Photovoltaic (PV) dataset [54] for solar power generations. (4) Power System Event Measurements. This is a 10-dimensional dataset (see Appendix B) produced by a high-order and time-dependent ODE system [55-57]. (5) Air Quality System. UCI Repository provides measurements of metal oxide chemical sensors in an air quality monitoring system [58]. (6) Electrocardiogram (ECG) signals. Recorded electrical signals from a patient's heart in the UCR Time Series Archive [59]. These test systems are representative, encompassing nonlinear and high-dimensional dynamics, as well as real-world applications in power systems, weather systems, and biomedical domains, all of which exhibit disturbances and noise. For these datasets, the interpolation and extrapolation tasks are illustrated in Appendix B.1. To evaluate these systems, we adopt a range of state-of-the-art methods based on Neural ODEs and Transformer, as detailed in Appendix C. Model architectures and training time comparisons are provided in Appendix D and Appendix E.3, respectively. For each method, we run 10 times and report the average errors.

4.1 Effective Symmetry Preservation in the Latent Space Z

First, we validate whether Latent MoS can correctly preserve the symmetry. We test the model in the ODE systems. As shown in the left part of Fig. 2, the true data are governed by linear or nonlinear rotational and slight scaling symmetry. Then, we set the data drop rate to be 90%. We utilize Principal Component Analysis to reduce the 15-dimensional latent vector (m = 15) in \mathcal{Z} to 2D for visualizations in the middle and right parts of Fig. 2. The result suggests that even with limited input data, latent MoS captures the correct and highly interpretable latent geometry, which can be used for the geometry-based analyses in dynamical systems. However, Latent ODE will produce unstructured latent trajectories that risk overfitting. The predicted curve visualizations are provided in Appendix E.2.

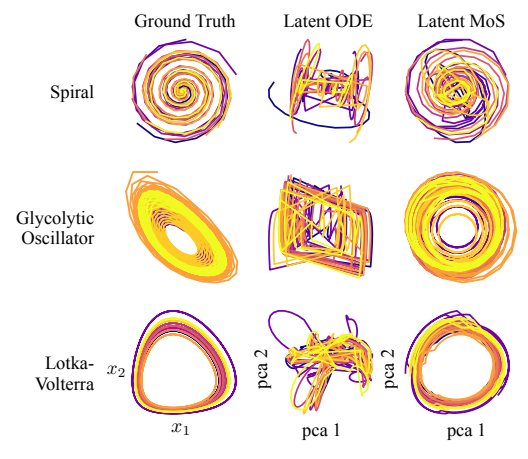


Figure 2: Raw data (left) and latent trajectories for Latent ODE (middle) and Latent MoS (right).

In the Glycolytic system, even when all symmetry experts are included, the model achieves a low MSE of 0.0033. Importantly, the gating weights are highly concentrated: the dominant expert, i.e., a second-order transformation (rotation \times scaling), receives a weight of 0.97, while the next highest (scaling \times rotation) receives 0.025, and the remaining experts collectively contribute less

Table 1: Test Mean Squared Error	MSF)	$(\times 10^{-2})$	for extra	nolation tasks	under varving	dron rates
Table 1. Test Mean Squared Effor	(TATOLT) ($(\Delta 10)$	ioi exua	poiation tasks	unuci vai yiii;	g urop raies.

Data	Drop	EqSINDy	EqGP	RNN- Δ_t	ODE-RNN	NCDE	Contiformer	Informer	Autoformer	Latent ODE	Latent MoS
	90%	1.79	2.01	1.01	1.16	1.34	1.07	1.21	1.13	1.04	0.62
Spiral	60%	0.88	0.96	0.49	0.98	1.31	1.09	1.09	0.89	0.99	0.54
•	30%	0.45	0.78	0.33	0.95	1.11	1.09	1.10	0.93	0.96	0.33
	90%	10.23	13.12	0.52	13.44	12.11	13.57	12.92	2.47	9.88	0.32
Glycolytic	60%	8.81	13.06	0.20	13.29	11.23	7.54	0.77	0.49	3.88	0.15
	30%	8.97	10.98	0.33	13.28	11.10	3.51	0.06	0.16	2.67	0.06
	90%	8.70	10.66	0.81	5.39	13.49	6.30	14.50	6.55	0.43	0.61
Lotka	60%	5.34	11.23	0.75	5.35	12.28	4.25	14.51	5.48	0.18	0.13
	30%	3.98	10.75	0.35	5.32	11.10	2.49	14.50	1.80	0.09	0.05
	90%	7.88	7.67	8.69	8.01	18.39	10.57	8.70	18.13	5.18	3.25
Load	60%	4.98	4.27	5.75	6.39	15.19	5.49	8.39	9.81	3.61	2.42
	30%	3.14	3.06	5.10	5.93	11.19	5.14	7.89	6.27	2.96	1.33
	90%	20.13	22.98	17.16	10.53	25.33	19.82	24.50	20.44	11.26	8.83
Solar	60%	21.25	20.41	12.77	7.62	24.19	17.43	15.58	15.23	8.17	5.01
	30%	16.82	18.37	11.38	7.36	19.84	15.53	15.31	16.08	7.28	3.48
	90%	7.72	8.21	8.04	9.43	10.45	8.09	10.05	8.65	8.02	5.32
Power event	60%	6.43	8.89	7.95	8.84	9.08	7.23	8.17	7.85	6.98	3.75
	30%	5.89	5.62	7.69	8.41	8.98	6.74	7.22	7.58	6.78	2.53
	90%	10.09	9.22	9.38	10.50	11.20	8.44	8.28	10.56	9.55	5.90
Air quality	60%	10.07	8.71	8.91	8.86	10.59	7.11	10.38	12.21	7.89	4.10
	30%	9.13	8.98	7.95	6.91	9.05	6.89	7.99	9.44	6.40	2.69
	90%	5.98	6.92	3.48	4.33	5.33	3.49	4.08	3.91	3.04	1.08
ECG	60%	5.13	5.12	2.02	3.23	4.59	2.13	2.11	4.10	1.03	0.91
	30%	4.29	3.77	1.84	2.70	4.19	1.04	1.49	3.48	1.02	0.62

than 0.005. This concentration indicates that the model identifies and relies on the correct symmetry transformation.

4.2 Overall Evaluations on Diverse Datasets with Different Data Drop Rates

We evaluate the model performance under varying drop rates: 90%, 60%, and 30%. The complete results are shown in Fig. 3 (see also Table 3 in Appendix E.1) for interpolation tasks and Table 1 for extrapolation tasks. In general, Contiformer, Latent ODE, and the proposed Latent MoS all achieve strong performance across both continuous ODE-based systems and real-world datasets with high disturbances. This is attributed to their shared ability to reconstruct latent trajectories during decoding, effectively capturing the underlying system dynamics. Among them, Latent MoS leverages geometric priors to structure the latent trajectories (see Fig. 2). For instance, while Contiformer and Latent ODE struggle with high-frequency Glycolytic oscillations, Latent MoS successfully encodes the data into a latent space $\mathcal Z$ where linear Lie group action-based dynamics can be more easily estimated. Across all datasets, Latent MoS achieves relative improvements ranging from 15% to 97%. In contrast, Informer and Autoformer only perform well under low drop rates, as they rely on pre-interpolation and lack the capacity to model the underlying continuous dynamics directly.

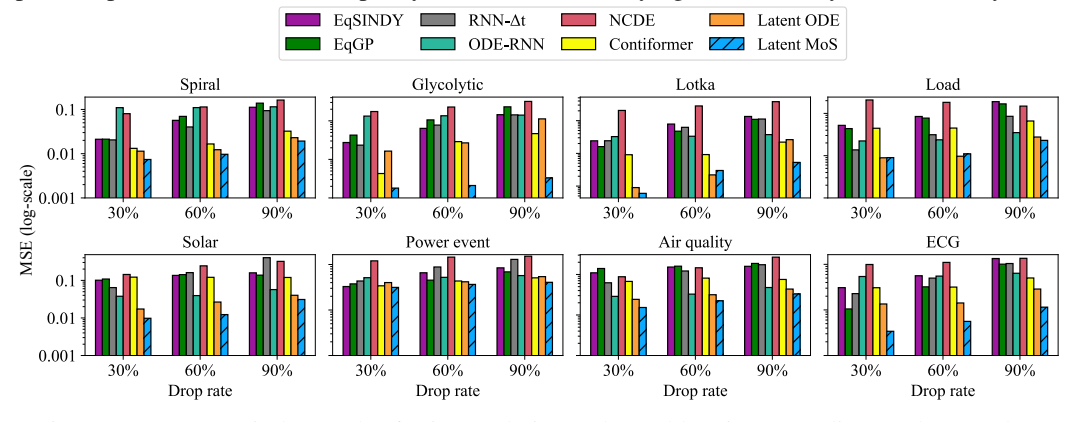


Figure 3: Test MSE in log-scales for interpolation tasks. Table 3 in Appendix E.1 shows values.

4.3 Sensitivity Analysis on Noise, Gating Mechanisms, and Latent Dimensionality

We use the Glycolytic system as an example for sensitivity analysis under a 90% data drop rate. Similar trends are observed across other systems. Fig. 4 shows the interpolation test set MSE under

various conditions. First, we introduce Gaussian noise with increasing standard deviations. The MSE for both Latent ODE and Latent MoS rises gradually, reflecting the impact of noise. This demonstrates that they are robust to noise perturbations and capable of approximating the underlying average trend. Second, we vary the latent dimensionality m. Latent MoS exhibits a sharp drop in MSE when m > 5. This suggests that a higher m provides sufficient capacity for approximating the nonlinear Lie group actions described in Equation (2), while still preserving linear operations within \mathcal{Z} . In contrast, Latent ODE lacks structured inductive biases in its latent space, and its performance remains relatively unaffected by increased dimensionality. Third, we examine the effect of the gating mechanism by allowing the top $K_0 \leq K$ gates with the highest scores to open and vary K_0 . The error remains when $K_0 \in [1,4]$ because Glycolytic system contains rotational and scaling symmetries. However, when K_0 becomes large, Latent MoS tends to overfit. Empirically, we find that setting $K_0 = 4$ yields strong performance, though further improvements can be achieved through hyperparameter tuning.

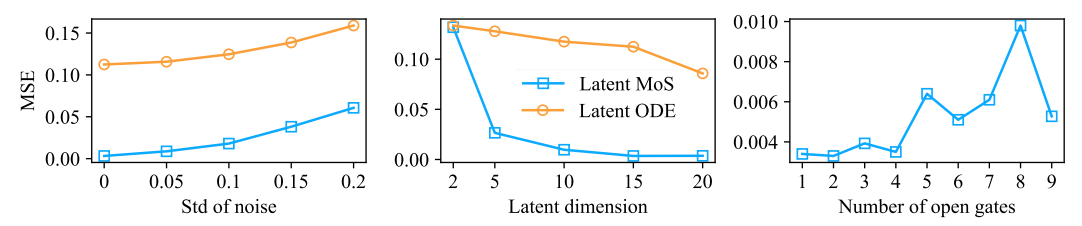


Figure 4: Results in sensitivity analysis for Glycolytic systems under 90% data drops.

Scalability in high-dimensional systems. Consistent with empirical findings in Latent ODEs [18], we observe that Latent MoS achieves strong performance on the 10-dimensional power event dataset by setting m=30. We hypothesize that this efficiency stems from underlying physical correlations.

4.4 Ablation Study

Using the same setting as in Section 4.3, we conduct an ablation study. As shown in Fig. 5, the presence of sparse gates is crucial for selecting relevant symmetries in our MoS framework. Furthermore, in the Glycolytic system, removing scaling or rotational symmetries significantly increases the MSE. Interestingly, performance improves when unnecessary symmetries, such as translational or certain second-order components, are excluded. When the translational expert is removed (which is unnecessary for Glycolytic dynamics), the MSE decreases to 0.001 and the gating weight for rotation × scaling increases to 0.99.

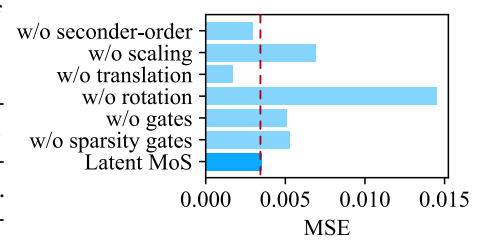


Figure 5: Results in ablation studies.

This demonstrates that while the gating works well, a simplified expert set can enhance efficiency and robustness. To achieve the best performance, we can perform a validation-based procedure to progressively remove unnecessary experts and compare the resulting MSE. Importantly, the gating mechanism remains valuable in this process: it helps identify the dominant expert(s) within a candidate subset, effectively narrowing down the search space.

4.5 Dynamic Learning for Control

We introduce an optimal frequency control problem in power systems. The task is to stabilize the generator's frequency. Past methods [60] assume an idealistic second-order ODE model, i.e., swing equations, to model frequency dynamics. However, real-world dynamics are higher-order with unknown physical parameters. Hence, we utilize latent MoS to learn it. In general, we compare model-free proximal policy optimization (PPO) [61], model-based policy optimization (MBPO) with a Gaussian process (MBPO-GP) [62], MBPO with Latent MoS (MBPO-MoS), and MBPO with the swing equation (MBPO-SE). By the end time, our MBPO-MoS stabilizes near zero with a deviation -0.024, the lowest among all methods. In contrast, PPO remains highly unstable (-0.928), MBPO-GP yields 0.100, and MBPO-SE yields -0.115. The general cost (integral of the Euclidean norm of frequency deviations) in the control process is 0.081 (MBPO-MoS), 0.163 (MBPO-SE), 0.257 (MBPO-GP), and 0.51 (PPO). Our learned dynamics in Latent MoS can much better predict the future frequency, hence largely improving control performance.

5 Related Work

Dynamic Modeling Against Data Scarcity. Existing approaches to dynamic modeling under data scarcity fall into four categories. The first focuses on interpolation: model-based methods (e.g., multidimensional interpolation [63], physical estimations [64]) assume explicit system behavior, while optimization-based techniques (e.g., compressed sensing [8], matrix completion [15]) rely on low-rank or sparsity assumptions to ensure tractability. Data-driven models from signal processing and machine learning [65, 12] can adapt to complex patterns but often neglect domain-specific structures. The second category incorporates physical knowledge through governing equations [11, 12, 66], enabling convergence even from sparse data. The third uses Bayesian inference to inject priors and quantify uncertainty [13–15], though performance depends heavily on prior quality. The fourth employs neural ODE solvers [16], including Latent ODEs [18] and Neural CDEs [17], which model latent continuous-time flows decodable to system states but require high-resolution data, as ODE integral errors accumulate [67].

Symmetry-based Learning. Enforcing symmetry priors in equivariant neural networks improves generalization and sample efficiency for applications like image processing [27–30] and RL [31–33]. However, they typically demand prior knowledge to handcraft symmetry transformations. To discover unknown symmetry knowledge, pioneer work involves a restrictive search space [68–70, 42, 38], e.g., a discrete symmetry group [39]. Recent work extends this study to generate and approximate different kinds of symmetries [40, 41, 37]. In particular, the framework based on Generative Adversarial Networks (GANs) [40, 41, 37] is highly generalizable to finding different symmetries in the latent space, grounded on the theory of Lie algebra. Nevertheless, GAN is known to have training instability [71], and their methods may deliver fallacious, trivial, or unclear solutions [41].

Symmetry-breaking Learning. Existing approaches that incorporate symmetry breaking in machine learning can be categorized into three main groups. (1) Learnable or non-stationary weights relax strict equivariance by allowing model parameters to adapt locally [44–46]. (2) Soft regularization encourages but does not strictly enforce equivariance, typically through auxiliary loss terms [43]. (3) Symmetry-breaking sets provide a constructive strategy by introducing minimal auxiliary inputs to selectively break output symmetry [72]. Our model falls into the first category, employing locally adaptive, learnable weights to capture approximate symmetries.

6 Conclusion, Limitation, and Future Work

We present Latent MoS, a sample-efficient framework for learning dynamical systems that explicitly preserves equivariance through structured latent transformations. Motivated by the observation that real-world systems often exhibit symmetry breaking, where strict group invariances hold only approximately or locally, Latent MoS captures these effects through mixtures of symmetry groups and adaptable latent flows. Grounded in Lie group theory, our approach provides a physically interpretable and effective means of modeling system dynamics under symmetry constraints. Although the set of predefined candidate transformations does not cover the full space of possible Lie group representations, empirical results demonstrate consistent improvements across a wide range of physical systems. The modular design of Latent MoS further enables natural extensions to incorporate additional or more complex symmetry transformations.

Latent MoS is primarily suited for systems that exhibit at least local symmetries. While systems entirely lacking symmetry, such as highly chaotic or purely stochastic processes (e.g., unconstrained turbulence), may fall outside its intended scope, such cases are rare in practice. Most real-world physical, biological, and engineered systems exhibit local or approximate symmetries due to conservation laws, structural regularities, or recurring patterns.

In future work, we plan to extend Latent MoS in two directions. First, we will develop automated mechanisms to refine and constrain the candidate set of symmetries, using validation-based selection or search strategies, so that the model can achieve the best performance even when the true symmetries are uncertain. Second, we aim to explore physically meaningful symmetry structures for broader geometric analyses in dynamical systems, including stability, safety, and contraction properties.

References

- [1] Haoran Li and Yang Weng. Physical equation discovery using physics-consistent neural network (pcnn) under incomplete observability. In *Proceedings of the 27th ACM SIGKDD Conference on Knowledge Discovery & Data Mining*, pages 925–933, 2021.
- [2] Haoran Li, Yang Weng, and Hanghang Tong. Console: Convex neural symbolic learning. *Advances in Neural Information Processing Systems*, 35:5766–5774, 2022.
- [3] Anusha Nagabandi, Gregory Kahn, Ronald S. Fearing, and Sergey Levine. Neural network dynamics for model-based deep reinforcement learning with model-free fine-tuning. In 2018 IEEE International Conference on Robotics and Automation (ICRA), pages 7559–7566, 2018.
- [4] Felix Berkenkamp, Matteo Turchetta, Angela Schoellig, and Andreas Krause. Safe model-based reinforcement learning with stability guarantees. *Advances in neural information processing systems*, 30, 2017.
- [5] Wenqi Cui and Baosen Zhang. Lyapunov-regularized reinforcement learning for power system transient stability. *IEEE Control Systems Letters*, 6:974–979, 2021.
- [6] Jian Li, Ming Zhao, and Kai Zhang. Low-quality and missing data handling in power grids using neural networks. *IEEE Transactions on Smart Grid*, 2024. to appear.
- [7] Chenhan Xiao, Yizheng Liao, and Yang Weng. Distribution grid line outage identification with unknown pattern and performance guarantee. *IEEE Transactions on Power Systems*, 2023.
- [8] David L Donoho. Compressed sensing. IEEE Transactions on information theory, 52(4):1289– 1306, 2006.
- [9] Yuejie Chi, Yue M Lu, and Yuxin Chen. Nonconvex optimization meets low-rank matrix factorization: An overview. *IEEE Transactions on Signal Processing*, 67(20):5239–5269, 2019.
- [10] Mark A Iwen, Felix Krahmer, Sara Krause-Solberg, and Johannes Maly. On recovery guarantees for one-bit compressed sensing on manifolds. *Discrete & computational geometry*, 65:953–998, 2021.
- [11] Zhao Chen, Yang Liu, and Hao Sun. Physics-informed learning of governing equations from scarce data. *Nature communications*, 12(1):6136, 2021.
- [12] Haoran Li, Zhihao Ma, Yang Weng, Haiwang Zhong, and Xiaodong Zheng. Low-dimensional ode embedding to convert low-resolution meters into "virtual" pmus. *IEEE Transactions on Power Systems*, pages 1–13, 2024.
- [13] Jesper Kjær Nielsen, Mads Græsbøll Christensen, A Taylan Cemgil, Simon J Godsill, and Søren Holdt Jensen. Bayesian interpolation and parameter estimation in a dynamic sinusoidal model. *IEEE transactions on audio, speech, and language processing*, 19(7):1986–1998, 2011.
- [14] Nathaniel J Linden, Boris Kramer, and Padmini Rangamani. Bayesian parameter estimation for dynamical models in systems biology. *PLoS computational biology*, 18(10):e1010651, 2022.
- [15] Ming Yi, Meng Wang, Tianqi Hong, and Dongbo Zhao. Bayesian high-rank hankel matrix completion for nonlinear synchrophasor data recovery. *IEEE Transactions on Power Systems*, 2023.
- [16] Ricky TQ Chen, Yulia Rubanova, Jesse Bettencourt, and David K Duvenaud. Neural ordinary differential equations. In Advances in Neural Information Processing Systems, pages 6571–6583, 2018.
- [17] Patrick Kidger, James Morrill, James Foster, and Terry Lyons. Neural controlled differential equations for irregular time series. *Advances in Neural Information Processing Systems*, 33:6696–6707, 2020.
- [18] Yulia Rubanova, Ricky TQ Chen, and David K Duvenaud. Latent ordinary differential equations for irregularly-sampled time series. Advances in neural information processing systems, 32, 2019.

- [19] Haoran Li, Muhao Guo, Yang Weng, and Hanghang Tong. Neural predictive control to coordinate discrete-and continuous-time models for time-series analysis with control-theoretical improvements. *arXiv* preprint arXiv:2508.01833, 2025.
- [20] Emilien Dupont, Arnaud Doucet, and Yee Whye Teh. Augmented neural odes. *Advances in neural information processing systems*, 32, 2019.
- [21] Giovanni Russo and Jean-Jacques E Slotine. Symmetries, stability, and control in nonlinear systems and networks. *Physical Review E—Statistical, Nonlinear, and Soft Matter Physics*, 84(4):041929, 2011.
- [22] Shengchao Yan, Baohe Zhang, Yuan Zhang, Joschka Boedecker, and Wolfram Burgard. Learning continuous control with geometric regularity from robot intrinsic symmetry. In 2024 IEEE International Conference on Robotics and Automation (ICRA), pages 49–55, 2024.
- [23] Congyue Deng, Or Litany, Yueqi Duan, Adrien Poulenard, Andrea Tagliasacchi, and Leonidas J. Guibas. Vector neurons: A general framework for so(3)-equivariant networks. In *Proceedings of the IEEE/CVF International Conference on Computer Vision (ICCV)*, pages 12200–12209, October 2021.
- [24] J Lewis Blackburn. Symmetrical components for power systems engineering. CRC press, 2017.
- [25] John David Crawford and Edgar Knobloch. Symmetry and symmetry-breaking bifurcations in fluid dynamics. Annual Review of Fluid Mechanics, 23(1):341–387, 1991.
- [26] Cristian-Ioan Vasile, Mac Schwager, and Calin Belta. Translational and rotational invariance in networked dynamical systems. *IEEE Transactions on Control of Network Systems*, 5(3):822– 832, 2018.
- [27] Victor Garcia Satorras, Emiel Hoogeboom, and Max Welling. E (n) equivariant graph neural networks. In *International conference on machine learning*, pages 9323–9332. PMLR, 2021.
- [28] Lingshen He, Yuxuan Chen, Yiming Dong, Yisen Wang, Zhouchen Lin, et al. Efficient equivariant network. *Advances in Neural Information Processing Systems*, 34:5290–5302, 2021.
- [29] David Ruhe, Johannes Brandstetter, and Patrick Forré. Clifford group equivariant neural networks. In A. Oh, T. Naumann, A. Globerson, K. Saenko, M. Hardt, and S. Levine, editors, *Advances in Neural Information Processing Systems*, volume 36, pages 62922–62990. Curran Associates, Inc., 2023.
- [30] Simon Batzner, Albert Musaelian, Lixin Sun, Mario Geiger, Jonathan P Mailoa, Mordechai Kornbluth, Nicola Molinari, Tess E Smidt, and Boris Kozinsky. E (3)-equivariant graph neural networks for data-efficient and accurate interatomic potentials. *Nature communications*, 13(1):2453, 2022.
- [31] Dian Wang, Robin Walters, and Robert Platt. So(2)-equivariant reinforcement learning. In *International Conference on Learning Representations*, 2022.
- [32] Arnab Kumar Mondal, Vineet Jain, Kaleem Siddiqi, and Siamak Ravanbakhsh. Eqr: Equivariant representations for data-efficient reinforcement learning. In *International Conference on Machine Learning*, pages 15908–15926. PMLR, 2022.
- [33] Joshua McClellan, Naveed Haghani, John Winder, Furong Huang, and Pratap Tokekar. Boosting sample efficiency and generalization in multi-agent reinforcement learning via equivariance. *arXiv preprint arXiv:2410.02581*, 2024.
- [34] Johannes Brandstetter, Max Welling, and Daniel E Worrall. Lie point symmetry data augmentation for neural pde solvers. In *International Conference on Machine Learning*, pages 2241–2256. PMLR, 2022.
- [35] In Huh, Eunho Yang, Sung Ju Hwang, and Jinwoo Shin. Time-reversal symmetric ode network. *Advances in Neural Information Processing Systems*, 33:19016–19027, 2020.

- [36] Tara Akhound-Sadegh, Laurence Perreault-Levasseur, Johannes Brandstetter, Max Welling, and Siamak Ravanbakhsh. Lie point symmetry and physics-informed networks. *Advances in Neural Information Processing Systems*, 36, 2024.
- [37] Jianke Yang, Wang Rao, Nima Dehmamy, Robin Walters, and Rose Yu. Symmetry-informed governing equation discovery. *arXiv preprint arXiv:2405.16756*, 2024.
- [38] Miguel Abreu, Luis Paulo Reis, and Nuno Lau. Addressing imperfect symmetry: a novel symmetry-learning actor-critic extension. *Neurocomputing*, 614:128771, 2025.
- [39] Pablo Calvo-Barlés, Sergio G Rodrigo, Eduardo Sánchez-Burillo, and Luis Martín-Moreno. Finding discrete symmetry groups via machine learning. *Physical Review E*, 110(4):045304, 2024.
- [40] Jianke Yang, Nima Dehmamy, Robin Walters, and Rose Yu. Latent space symmetry discovery. *arXiv preprint arXiv:2310.00105*, 2023.
- [41] Jianke Yang, Robin Walters, Nima Dehmamy, and Rose Yu. Generative adversarial symmetry discovery. In *International Conference on Machine Learning*, pages 39488–39508. PMLR, 2023.
- [42] Samuel E Otto, Nicholas Zolman, J Nathan Kutz, and Steven L Brunton. A unified framework to enforce, discover, and promote symmetry in machine learning. arXiv preprint arXiv:2311.00212, 2023.
- [43] Hyunsu Kim, Hyungi Lee, Hongseok Yang, and Juho Lee. Regularizing towards soft equivariance under mixed symmetries. In *International Conference on Machine Learning*, pages 16712–16727. PMLR, 2023.
- [44] Rui Wang, Robin Walters, and Rose Yu. Approximately equivariant networks for imperfectly symmetric dynamics. In *International Conference on Machine Learning*, pages 23078–23091. PMLR, 2022.
- [45] Rui Wang, Elyssa Hofgard, Han Gao, Robin Walters, and Tess E Smidt. Discovering symmetry breaking in physical systems with relaxed group convolution. *arXiv* preprint arXiv:2310.02299, 2023.
- [46] Tycho van der Ouderaa, David W Romero, and Mark van der Wilk. Relaxing equivariance constraints with non-stationary continuous filters. Advances in Neural Information Processing Systems, 35:33818–33830, 2022.
- [47] Alexander A Kirillov. *An introduction to Lie groups and Lie algebras*, volume 113. Cambridge University Press, 2008.
- [48] Josip Česić, Ivan Marković, and Ivan Petrović. Mixture reduction on matrix lie groups. *Ieee signal processing letters*, 24(11):1719–1723, 2017.
- [49] Saeed Masoudnia and Reza Ebrahimpour. Mixture of experts: a literature survey. *Artificial Intelligence Review*, 42:275–293, 2014.
- [50] Ernst Hairer, Marlis Hochbruck, Arieh Iserles, and Christian Lubich. Geometric numerical integration. *Oberwolfach Reports*, 3(1):805–882, 2006.
- [51] Marija Ilic, Le Xie, and Qixing Liu. *Engineering IT-enabled sustainable electricity services:* The tale of two low-cost green azores islands, volume 30. Springer, 2013.
- [52] Haoran Li, Muhao Guo, Marija Ilic, Yang Weng, and Guangchun Ruan. External dataenhanced meta-representation for adaptive probabilistic load forecasting. *arXiv* preprint arXiv:2506.23201, 2025.
- [53] Haoran Li, Muhao Guo, Yang Weng, Marija Ilic, and Guangchun Ruan. Exarnn: An environment-driven adaptive rnn for learning non-stationary power dynamics. arXiv preprint arXiv:2505.17488, 2025.

- [54] Matthew Boyd. Nist weather station for photovoltaic and building system research. *National Institute of Standards and Technology, Gaithersburg, MD, Technical Note*, (1913), 2016.
- [55] Haoran Li, Yang Weng, Evangelos Farantatos, and Mahendra Patel. An unsupervised learning framework for event detection, type identification and localization using pmus without any historical labels. In 2019 IEEE Power & Energy Society General Meeting (PESGM), pages 1–5, 2019.
- [56] Haoran Li, Yang Weng, Evangelos Farantatos, and Mahendra Patel. A hybrid machine learning framework for enhancing pmu-based event identification with limited labels. In 2019 International Conference on Smart Grid Synchronized Measurements and Analytics (SGSMA), pages 1–8, 2019.
- [57] Haoran Li, Zhihao Ma, Yang Weng, Erik Blasch, and Surya Santoso. Structural tensor learning for event identification with limited labels. *IEEE Transactions on Power Systems*, 38(6):5314– 5328, 2023.
- [58] Saverio Vito. Air Quality. UCI Machine Learning Repository, 2008. DOI: https://doi.org/10.24432/C59K5F.
- [59] Yanping Chen, Eamonn Keogh, Bing Hu, Nurjahan Begum, Anthony Bagnall, Abdullah Mueen, and Gustavo Batista. The ucr time series classification archive, July 2015. www.cs.ucr.edu/~eamonn/time_series_data/.
- [60] Hamad Alduaij, Yang Weng, and Haoran Li. Beyond monotonic droop: Expanding feasible control regions for optimal frequency regulation. *IEEE Transactions on Power Systems*, pages 1–14, 2025.
- [61] John Schulman, Filip Wolski, Prafulla Dhariwal, Alec Radford, and Oleg Klimov. Proximal policy optimization algorithms. arXiv preprint arXiv:1707.06347, 2017.
- [62] Marc Peter Deisenroth, Dieter Fox, and Carl Edward Rasmussen. Gaussian processes for data-efficient learning in robotics and control. *IEEE transactions on pattern analysis and machine intelligence*, 37(2):408–423, 2013.
- [63] Christian Habermann and Fabian Kindermann. Multidimensional spline interpolation: Theory and applications. *Computational Economics*, 30:153–169, 2007.
- [64] Mauricio D Sacchi, Tadeusz J Ulrych, and Colin J Walker. Interpolation and extrapolation using a high-resolution discrete fourier transform. *IEEE Transactions on Signal Processing*, 46(1):31–38, 1998.
- [65] Kai Fukami, Koji Fukagata, and Kunihiko Taira. Machine-learning-based spatio-temporal super resolution reconstruction of turbulent flows. *Journal of Fluid Mechanics*, 909:A9, 2021.
- [66] Yeonjong Shin, Jerome Darbon, and George Em Karniadakis. On the convergence of physics informed neural networks for linear second-order elliptic and parabolic type pdes. arXiv preprint arXiv:2004.01806, 2020.
- [67] Birgit Hillebrecht and Benjamin Unger. Certified machine learning: A posteriori error estimation for physics-informed neural networks. In 2022 International Joint Conference on Neural Networks (IJCNN), pages 1–8. IEEE, 2022.
- [68] Gregory Benton, Marc Finzi, Pavel Izmailov, and Andrew G Wilson. Learning invariances in neural networks from training data. Advances in neural information processing systems, 33:17605–17616, 2020.
- [69] Allan Zhou, Tom Knowles, and Chelsea Finn. Meta-learning symmetries by reparameterization. *arXiv preprint arXiv:2007.02933*, 2020.
- [70] David W Romero and Suhas Lohit. Learning partial equivariances from data. *Advances in Neural Information Processing Systems*, 35:36466–36478, 2022.

- [71] Lars Mescheder, Andreas Geiger, and Sebastian Nowozin. Which training methods for gans do actually converge? In *International conference on machine learning*, pages 3481–3490. PMLR, 2018.
- [72] YuQing Xie. Equivariant symmetry breaking sets. Massachusetts Institute of Technology, 2024.
- [73] Evgeni E SEL'KOV. Self-oscillations in glycolysis 1. a simple kinetic model. *European Journal of Biochemistry*, 4(1):79–86, 1968.
- [74] Haoran Li, Yang Weng, Evangelos Farantatos, and Mahendra Patel. An unsupervised learning framework for event detection, type identification and localization using pmus without any historical labels. In 2019 IEEE Power & Energy Society General Meeting (PESGM), pages 1–5. IEEE, 2019.
- [75] Haoran Li, Zhihao Ma, and Yang Weng. A transfer learning framework for power system event identification. *IEEE Transactions on Power Systems*, 37(6):4424–4435, 2022.
- [76] General Electric Energy Consulting. General Electric Concorda PSLF. 2018.
- [77] Engineering Texas A&M University. Illinois 200-Bus System: ACTIVSg200. 2016.
- [78] Dheeru Dua, Casey Graff, et al. Uci machine learning repository. 2017.
- [79] Zhengping Che, Sanjay Purushotham, Kyunghyun Cho, David Sontag, and Yan Liu. Recurrent neural networks for multivariate time series with missing values. *Scientific reports*, 8(1):1–12, 2018.
- [80] Yuqi Chen, Kan Ren, Yansen Wang, Yuchen Fang, Weiwei Sun, and Dongsheng Li. Contiformer: Continuous-time transformer for irregular time series modeling. *Advances in Neural Information Processing Systems*, 36, 2024.
- [81] Haoyi Zhou, Shanghang Zhang, Jieqi Peng, Shuai Zhang, Jianxin Li, Hui Xiong, and Wancai Zhang. Informer: Beyond efficient transformer for long sequence time-series forecasting. In *Proceedings of the AAAI conference on artificial intelligence*, volume 35, pages 11106–11115, 2021.
- [82] Haixu Wu, Jiehui Xu, Jianmin Wang, and Mingsheng Long. Autoformer: Decomposition transformers with auto-correlation for long-term series forecasting. *Advances in neural information processing systems*, 34:22419–22430, 2021.

NeurIPS Paper Checklist

The checklist is designed to encourage best practices for responsible machine learning research, addressing issues of reproducibility, transparency, research ethics, and societal impact. Do not remove the checklist: **The papers not including the checklist will be desk rejected.** The checklist should follow the references and follow the (optional) supplemental material. The checklist does NOT count towards the page limit.

Please read the checklist guidelines carefully for information on how to answer these questions. For each question in the checklist:

- You should answer [Yes], [No], or [NA].
- [NA] means either that the question is Not Applicable for that particular paper or the relevant information is Not Available.
- Please provide a short (1–2 sentence) justification right after your answer (even for NA).

The checklist answers are an integral part of your paper submission. They are visible to the reviewers, area chairs, senior area chairs, and ethics reviewers. You will be asked to also include it (after eventual revisions) with the final version of your paper, and its final version will be published with the paper.

The reviewers of your paper will be asked to use the checklist as one of the factors in their evaluation. While "[Yes]" is generally preferable to "[No]", it is perfectly acceptable to answer "[No]" provided a proper justification is given (e.g., "error bars are not reported because it would be too computationally expensive" or "we were unable to find the license for the dataset we used"). In general, answering "[No]" or "[NA]" is not grounds for rejection. While the questions are phrased in a binary way, we acknowledge that the true answer is often more nuanced, so please just use your best judgment and write a justification to elaborate. All supporting evidence can appear either in the main paper or the supplemental material, provided in appendix. If you answer [Yes] to a question, in the justification please point to the section(s) where related material for the question can be found.

IMPORTANT, please:

- Delete this instruction block, but keep the section heading "NeurIPS Paper Checklist",
- Keep the checklist subsection headings, questions/answers and guidelines below.
- Do not modify the questions and only use the provided macros for your answers.

1. Claims

Question: Do the main claims made in the abstract and introduction accurately reflect the paper's contributions and scope?

Answer: [Yes]

Justification: The material can be found in Abstract and Introduction.

Guidelines:

- The answer NA means that the abstract and introduction do not include the claims made in the paper.
- The abstract and/or introduction should clearly state the claims made, including the contributions made in the paper and important assumptions and limitations. A No or NA answer to this question will not be perceived well by the reviewers.
- The claims made should match theoretical and experimental results, and reflect how much the results can be expected to generalize to other settings.
- It is fine to include aspirational goals as motivation as long as it is clear that these goals are not attained by the paper.

2. Limitations

Question: Does the paper discuss the limitations of the work performed by the authors?

Answer: [Yes]

Justification: The discussion of limitations of the work can be found in Conclusion section.

Guidelines:

- The answer NA means that the paper has no limitation while the answer No means that the paper has limitations, but those are not discussed in the paper.
- The authors are encouraged to create a separate "Limitations" section in their paper.
- The paper should point out any strong assumptions and how robust the results are to violations of these assumptions (e.g., independence assumptions, noiseless settings, model well-specification, asymptotic approximations only holding locally). The authors should reflect on how these assumptions might be violated in practice and what the implications would be.
- The authors should reflect on the scope of the claims made, e.g., if the approach was only tested on a few datasets or with a few runs. In general, empirical results often depend on implicit assumptions, which should be articulated.
- The authors should reflect on the factors that influence the performance of the approach. For example, a facial recognition algorithm may perform poorly when image resolution is low or images are taken in low lighting. Or a speech-to-text system might not be used reliably to provide closed captions for online lectures because it fails to handle technical jargon.
- The authors should discuss the computational efficiency of the proposed algorithms and how they scale with dataset size.
- If applicable, the authors should discuss possible limitations of their approach to address problems of privacy and fairness.
- While the authors might fear that complete honesty about limitations might be used by reviewers as grounds for rejection, a worse outcome might be that reviewers discover limitations that aren't acknowledged in the paper. The authors should use their best judgment and recognize that individual actions in favor of transparency play an important role in developing norms that preserve the integrity of the community. Reviewers will be specifically instructed to not penalize honesty concerning limitations.

3. Theory assumptions and proofs

Question: For each theoretical result, does the paper provide the full set of assumptions and a complete (and correct) proof?

Answer: [Yes]

Justification: The assumption and proofs can be found in Appendix A.

Guidelines:

- The answer NA means that the paper does not include theoretical results.
- All the theorems, formulas, and proofs in the paper should be numbered and cross-referenced.
- All assumptions should be clearly stated or referenced in the statement of any theorems.
- The proofs can either appear in the main paper or the supplemental material, but if they appear in the supplemental material, the authors are encouraged to provide a short proof sketch to provide intuition.
- Inversely, any informal proof provided in the core of the paper should be complemented by formal proofs provided in appendix or supplemental material.
- Theorems and Lemmas that the proof relies upon should be properly referenced.

4. Experimental result reproducibility

Question: Does the paper fully disclose all the information needed to reproduce the main experimental results of the paper to the extent that it affects the main claims and/or conclusions of the paper (regardless of whether the code and data are provided or not)?

Answer: [Yes]

Justification: The dataset details can be found in Appendix B. The baseline details can be found in Appendix C. The details of experiment setting can be found in Appendix D.

Guidelines:

• The answer NA means that the paper does not include experiments.

- If the paper includes experiments, a No answer to this question will not be perceived well by the reviewers: Making the paper reproducible is important, regardless of whether the code and data are provided or not.
- If the contribution is a dataset and/or model, the authors should describe the steps taken to make their results reproducible or verifiable.
- Depending on the contribution, reproducibility can be accomplished in various ways. For example, if the contribution is a novel architecture, describing the architecture fully might suffice, or if the contribution is a specific model and empirical evaluation, it may be necessary to either make it possible for others to replicate the model with the same dataset, or provide access to the model. In general, releasing code and data is often one good way to accomplish this, but reproducibility can also be provided via detailed instructions for how to replicate the results, access to a hosted model (e.g., in the case of a large language model), releasing of a model checkpoint, or other means that are appropriate to the research performed.
- While NeurIPS does not require releasing code, the conference does require all submissions to provide some reasonable avenue for reproducibility, which may depend on the nature of the contribution. For example
 - (a) If the contribution is primarily a new algorithm, the paper should make it clear how to reproduce that algorithm.
- (b) If the contribution is primarily a new model architecture, the paper should describe the architecture clearly and fully.
- (c) If the contribution is a new model (e.g., a large language model), then there should either be a way to access this model for reproducing the results or a way to reproduce the model (e.g., with an open-source dataset or instructions for how to construct the dataset).
- (d) We recognize that reproducibility may be tricky in some cases, in which case authors are welcome to describe the particular way they provide for reproducibility. In the case of closed-source models, it may be that access to the model is limited in some way (e.g., to registered users), but it should be possible for other researchers to have some path to reproducing or verifying the results.

5. Open access to data and code

Question: Does the paper provide open access to the data and code, with sufficient instructions to faithfully reproduce the main experimental results, as described in supplemental material?

Answer: [Yes]

Justification: we will submit code and data as supplementary materials. After the review process, we will upload the code to Github.

Guidelines:

- The answer NA means that paper does not include experiments requiring code.
- Please see the NeurIPS code and data submission guidelines (https://nips.cc/public/guides/CodeSubmissionPolicy) for more details.
- While we encourage the release of code and data, we understand that this might not be possible, so "No" is an acceptable answer. Papers cannot be rejected simply for not including code, unless this is central to the contribution (e.g., for a new open-source benchmark).
- The instructions should contain the exact command and environment needed to run to reproduce the results. See the NeurIPS code and data submission guidelines (https://nips.cc/public/guides/CodeSubmissionPolicy) for more details.
- The authors should provide instructions on data access and preparation, including how
 to access the raw data, preprocessed data, intermediate data, and generated data, etc.
- The authors should provide scripts to reproduce all experimental results for the new proposed method and baselines. If only a subset of experiments are reproducible, they should state which ones are omitted from the script and why.
- At submission time, to preserve anonymity, the authors should release anonymized versions (if applicable).

• Providing as much information as possible in supplemental material (appended to the paper) is recommended, but including URLs to data and code is permitted.

6. Experimental setting/details

Question: Does the paper specify all the training and test details (e.g., data splits, hyperparameters, how they were chosen, type of optimizer, etc.) necessary to understand the results?

Answer: [Yes]

Justification: The details of experiment setting can be found in Appendix D.

Guidelines:

- The answer NA means that the paper does not include experiments.
- The experimental setting should be presented in the core of the paper to a level of detail that is necessary to appreciate the results and make sense of them.
- The full details can be provided either with the code, in appendix, or as supplemental
 material.

7. Experiment statistical significance

Question: Does the paper report error bars suitably and correctly defined or other appropriate information about the statistical significance of the experiments?

Answer: [Yes]

Justification: The statistical errors are reported in Experiments, showing significant improvements in our methods.

Guidelines:

- The answer NA means that the paper does not include experiments.
- The authors should answer "Yes" if the results are accompanied by error bars, confidence intervals, or statistical significance tests, at least for the experiments that support the main claims of the paper.
- The factors of variability that the error bars are capturing should be clearly stated (for example, train/test split, initialization, random drawing of some parameter, or overall run with given experimental conditions).
- The method for calculating the error bars should be explained (closed form formula, call to a library function, bootstrap, etc.)
- The assumptions made should be given (e.g., Normally distributed errors).
- It should be clear whether the error bar is the standard deviation or the standard error
 of the mean.
- It is OK to report 1-sigma error bars, but one should state it. The authors should preferably report a 2-sigma error bar than state that they have a 96% CI, if the hypothesis of Normality of errors is not verified.
- For asymmetric distributions, the authors should be careful not to show in tables or figures symmetric error bars that would yield results that are out of range (e.g. negative error rates).
- If error bars are reported in tables or plots, The authors should explain in the text how they were calculated and reference the corresponding figures or tables in the text.

8. Experiments compute resources

Question: For each experiment, does the paper provide sufficient information on the computer resources (type of compute workers, memory, time of execution) needed to reproduce the experiments?

Answer: [Yes]

Justification: The resource is described in Appendix D, and the run time is described in Appendix E.3.

Guidelines:

• The answer NA means that the paper does not include experiments.

- The paper should indicate the type of compute workers CPU or GPU, internal cluster, or cloud provider, including relevant memory and storage.
- The paper should provide the amount of compute required for each of the individual experimental runs as well as estimate the total compute.
- The paper should disclose whether the full research project required more compute than the experiments reported in the paper (e.g., preliminary or failed experiments that didn't make it into the paper).

9. Code of ethics

Question: Does the research conducted in the paper conform, in every respect, with the NeurIPS Code of Ethics https://neurips.cc/public/EthicsGuidelines?

Answer: [Yes]

Justification: We have carefully read the codes and make sure it's well conducted.

Guidelines:

- The answer NA means that the authors have not reviewed the NeurIPS Code of Ethics.
- If the authors answer No, they should explain the special circumstances that require a
 deviation from the Code of Ethics.
- The authors should make sure to preserve anonymity (e.g., if there is a special consideration due to laws or regulations in their jurisdiction).

10. Broader impacts

Question: Does the paper discuss both potential positive societal impacts and negative societal impacts of the work performed?

Answer: [NA]

Justification: [TODO]

Guidelines:

- The answer NA means that there is no societal impact of the work performed.
- If the authors answer NA or No, they should explain why their work has no societal impact or why the paper does not address societal impact.
- Examples of negative societal impacts include potential malicious or unintended uses (e.g., disinformation, generating fake profiles, surveillance), fairness considerations (e.g., deployment of technologies that could make decisions that unfairly impact specific groups), privacy considerations, and security considerations.
- The conference expects that many papers will be foundational research and not tied to particular applications, let alone deployments. However, if there is a direct path to any negative applications, the authors should point it out. For example, it is legitimate to point out that an improvement in the quality of generative models could be used to generate deepfakes for disinformation. On the other hand, it is not needed to point out that a generic algorithm for optimizing neural networks could enable people to train models that generate Deepfakes faster.
- The authors should consider possible harms that could arise when the technology is being used as intended and functioning correctly, harms that could arise when the technology is being used as intended but gives incorrect results, and harms following from (intentional or unintentional) misuse of the technology.
- If there are negative societal impacts, the authors could also discuss possible mitigation strategies (e.g., gated release of models, providing defenses in addition to attacks, mechanisms for monitoring misuse, mechanisms to monitor how a system learns from feedback over time, improving the efficiency and accessibility of ML).

11. Safeguards

Question: Does the paper describe safeguards that have been put in place for responsible release of data or models that have a high risk for misuse (e.g., pretrained language models, image generators, or scraped datasets)?

Answer: [NA]

Justification: [TODO]

Guidelines:

- The answer NA means that the paper poses no such risks.
- Released models that have a high risk for misuse or dual-use should be released with necessary safeguards to allow for controlled use of the model, for example by requiring that users adhere to usage guidelines or restrictions to access the model or implementing safety filters.
- Datasets that have been scraped from the Internet could pose safety risks. The authors should describe how they avoided releasing unsafe images.
- We recognize that providing effective safeguards is challenging, and many papers do not require this, but we encourage authors to take this into account and make a best faith effort.

12. Licenses for existing assets

Question: Are the creators or original owners of assets (e.g., code, data, models), used in the paper, properly credited and are the license and terms of use explicitly mentioned and properly respected?

Answer: [NA]

Justification: [TODO]

Guidelines:

- The answer NA means that the paper does not use existing assets.
- The authors should cite the original paper that produced the code package or dataset.
- The authors should state which version of the asset is used and, if possible, include a
- The name of the license (e.g., CC-BY 4.0) should be included for each asset.
- For scraped data from a particular source (e.g., website), the copyright and terms of service of that source should be provided.
- If assets are released, the license, copyright information, and terms of use in the package should be provided. For popular datasets, paperswithcode.com/datasets has curated licenses for some datasets. Their licensing guide can help determine the license of a dataset.
- For existing datasets that are re-packaged, both the original license and the license of the derived asset (if it has changed) should be provided.
- If this information is not available online, the authors are encouraged to reach out to the asset's creators.

13. New assets

Question: Are new assets introduced in the paper well documented and is the documentation provided alongside the assets?

Answer: [NA]

Justification: [TODO]

Guidelines:

- The answer NA means that the paper does not release new assets.
- Researchers should communicate the details of the dataset/code/model as part of their submissions via structured templates. This includes details about training, license, limitations, etc.
- The paper should discuss whether and how consent was obtained from people whose asset is used.
- At submission time, remember to anonymize your assets (if applicable). You can either create an anonymized URL or include an anonymized zip file.

14. Crowdsourcing and research with human subjects

Question: For crowdsourcing experiments and research with human subjects, does the paper include the full text of instructions given to participants and screenshots, if applicable, as well as details about compensation (if any)?

Answer: [NA]

Justification: [TODO]

Guidelines:

- The answer NA means that the paper does not involve crowdsourcing nor research with human subjects.
- Including this information in the supplemental material is fine, but if the main contribution of the paper involves human subjects, then as much detail as possible should be included in the main paper.
- According to the NeurIPS Code of Ethics, workers involved in data collection, curation, or other labor should be paid at least the minimum wage in the country of the data collector.

15. Institutional review board (IRB) approvals or equivalent for research with human subjects

Question: Does the paper describe potential risks incurred by study participants, whether such risks were disclosed to the subjects, and whether Institutional Review Board (IRB) approvals (or an equivalent approval/review based on the requirements of your country or institution) were obtained?

Answer: [NA]

Justification: [TODO]

Guidelines:

- The answer NA means that the paper does not involve crowdsourcing nor research with human subjects.
- Depending on the country in which research is conducted, IRB approval (or equivalent)
 may be required for any human subjects research. If you obtained IRB approval, you
 should clearly state this in the paper.
- We recognize that the procedures for this may vary significantly between institutions and locations, and we expect authors to adhere to the NeurIPS Code of Ethics and the guidelines for their institution.
- For initial submissions, do not include any information that would break anonymity (if applicable), such as the institution conducting the review.

16. Declaration of LLM usage

Question: Does the paper describe the usage of LLMs if it is an important, original, or non-standard component of the core methods in this research? Note that if the LLM is used only for writing, editing, or formatting purposes and does not impact the core methodology, scientific rigorousness, or originality of the research, declaration is not required.

Answer: [NA]

Justification: [TODO]

Guidelines:

- The answer NA means that the core method development in this research does not involve LLMs as any important, original, or non-standard components.
- Please refer to our LLM policy (https://neurips.cc/Conferences/2025/LLM) for what should or should not be described.

Impact Statement

This paper presents work whose goal is to advance the field of Machine Learning. There are many potential societal consequences of our work, none which we feel must be specifically highlighted here.

A Detailed Proofs

A.1 Proof of Lemma 1

Lemma 1. Assume that G and $H \subseteq G$ are Lie groups whose elements are defined in Equation (6) and Equation (3), respectively. Define the centralizer of H in G as: $C_G(h) := \{g \in G | \pi_s(g)\pi_d(h) = \pi_d(h)\pi_s(g)\}$. If $C_G(h)$ is nontrivial (i.e., it contains elements other than the identity), then $\forall g \in C_G(h)$, the relation for $\pi_s(g)$ in Equation (3) is preserved.

Proof. For $\forall g \in C_G(h)$, we have

$$\pi_s(g)\mathbf{z}(t_{i+1}) = \pi_s(g)\pi_d(h)\mathbf{z}(t_i)$$
(11)

$$= \pi_d(h)\pi_s(g)\mathbf{z}(t_i) \tag{12}$$

$$= f_z(\pi_s(g)\mathbf{z}(t_i)), \tag{13}$$

where the first equality follows from Equation (6), the second by the definition of the centralizer, and the third again by Equation (6). \Box

A.2 Proof of Proposition 1

Proposition 1 (Sufficient Conditions for Nontrivial Centralizer). *Let* $H \subset \text{Aff}(m)$ *be a Lie subgroup whose elements are represented in homogeneous coordinates as affine transformations:*

$$\pi_d(h)\tilde{\boldsymbol{z}}(t) = \pi_d(h)\begin{pmatrix} \boldsymbol{z}(t) \\ 1 \end{pmatrix} = \begin{bmatrix} A_h & \boldsymbol{b}_h \\ \mathbf{0} & 1 \end{bmatrix} \begin{bmatrix} \boldsymbol{z}(t) \\ 1 \end{bmatrix}, \tag{14}$$

where $A_h \in GL(m)$, $\mathbf{b}_h \in \mathbb{R}^m$, and we use $\tilde{\mathbf{z}}(t) = [\mathbf{z}(t), 1]^{\top} \in \mathbb{R}^{m+1}$ to denote the augmented latent vector in homogeneous coordinates to support affine transformations. Suppose that for $\forall g, h \in H$, it holds that $A_g A_h = A_h A_g$ and $A_g \mathbf{b}_h = \mathbf{b}_h$. Then we have $H \subseteq C_G(h)$. In particular, $C_G(h)$ is nontrivial and contains at least all of elements in H.

Proof. We notice that

$$\pi_d(g)\,\pi_d(h) = \begin{bmatrix} A_g & \boldsymbol{b}_g \\ \boldsymbol{0} & 1 \end{bmatrix} \begin{bmatrix} A_h & \boldsymbol{b}_h \\ \boldsymbol{0} & 1 \end{bmatrix} = \begin{bmatrix} A_g A_h & A_g \boldsymbol{b}_h + \boldsymbol{b}_g \\ \boldsymbol{0} & 1 \end{bmatrix},\tag{15}$$

and

$$\pi_d(h) \, \pi_d(g) = \begin{bmatrix} A_h & \boldsymbol{b}_h \\ \boldsymbol{0} & 1 \end{bmatrix} \begin{bmatrix} A_g & \boldsymbol{b}_g \\ \boldsymbol{0} & 1 \end{bmatrix} = \begin{bmatrix} A_h A_g & A_h \boldsymbol{b}_g + \boldsymbol{b}_h \\ \boldsymbol{0} & 1 \end{bmatrix}. \tag{16}$$

Since for $\forall g, h \in H$, $A_g A_h = A_h A_g$ and $A_g \mathbf{b}_h = \mathbf{b}_h$, then we have $\pi_d(g) \pi_d(h) = \pi_d(h) \pi_d(g)$. It shows that every pair of elements $g, h \in H$ commute under π_d . Thus, $g \in C_G(h), \forall g \in H$. Thus, the centralizer is nontrivial and contains at least H.

A.3 Proof of Corollary 1

Corollary 1 (Equivariance of Planar Rotation Transformation). Let u_1 and u_2 be orthonormal vectors and $P := \begin{bmatrix} u_1 & u_2 \end{bmatrix} \in \mathbb{R}^{m \times 2}$. Consider the planar rotation transformation: $\hat{\pi}^{rot} = \begin{bmatrix} I_m + P(R_{\theta} - I_2)P^{\top} & 0 \\ 0 & 1 \end{bmatrix}$, where $R_{\theta} = \begin{bmatrix} \cos \theta & -\sin \theta \\ \sin \theta & \cos \theta \end{bmatrix} \in SO(2)$, I_m is the $m \times m$ identify matrix. Then, $\hat{\pi}^{rot}$ and its Lie group $H \subset SO(m)$ satisfies the conditions in Proposition 1.

Proof. For the rotation matrix $Q_{\theta} = I_m + P(R_{\theta} - I_2)P^{\top}$, we have

$$Q_{\theta}Q_{\gamma} = (I_m + P(R_{\theta} - I_2)P^{\top})(I_m + P(R_{\gamma} - I_2)P^{\top})$$

$$= I_m + P(R_{\theta} - I_2)P^{\top}P(R_{\gamma} - I_2)P^{\top} + P(R_{\theta} - I_2)P^{\top} + P(R_{\gamma} - I_2)P^{\top}$$

$$= I_m + P(R_{\theta} - I_2)(R_{\gamma} - I_2)P^{\top} + P(R_{\theta} - I_2)P^{\top} + P(R_{\gamma} - I_2)P^{\top}$$

and

$$Q_{\gamma}Q_{\theta} = (I_m + P(R_{\gamma} - I_2)P^{\top})(I_m + P(R_{\theta} - I_2)P^{\top})$$

= $I_m + P(R_{\gamma} - I_2)P^{\top}P(R_{\theta} - I_2)P^{\top} + P(R_{\gamma} - I_2)P^{\top} + P(R_{\theta} - I_2)P^{\top}$
= $I_m + P(R_{\gamma} - I_2)(R_{\theta} - I_2)P^{\top} + P(R_{\gamma} - I_2)P^{\top} + P(R_{\theta} - I_2)P^{\top}$.

where the equality holds due to $P^{\top}P = I_2$. Since we have

$$R_{\theta}R_{\gamma} = \begin{bmatrix} \cos \theta & -\sin \theta \\ \sin \theta & \cos \theta \end{bmatrix} \begin{bmatrix} \cos \gamma & -\sin \gamma \\ \sin \gamma & \cos \gamma \end{bmatrix} = \begin{bmatrix} \cos \theta \cos \gamma - \sin \theta \sin \gamma & -\cos \theta \sin \gamma - \sin \theta \cos \gamma \\ \sin \theta \cos \gamma + \cos \theta \sin \gamma & -\sin \theta \sin \gamma + \cos \theta \cos \gamma \end{bmatrix}$$
$$= \begin{bmatrix} \cos(\theta + \gamma) & -\sin(\theta + \gamma) \\ \sin(\theta + \gamma) & \cos(\theta + \gamma) \end{bmatrix} = R_{\theta + \gamma} = R_{\gamma}R_{\theta},$$

we also have $Q_{\theta}Q_{\gamma} = Q_{\gamma}Q_{\theta}$.

A.4 Proof of Corollary 2

Corollary 2 (Equivariance of Translation and Scaling Transformation). Denote the translation dynamics: $\hat{\pi}^{tra} = \begin{bmatrix} I_m & \mathbf{v} \\ \mathbf{0} & 1 \end{bmatrix}$ and its Lie group $H \subset E(m)$, where E(m) is an Euclidean group.

They satisfy the conditions in Proposition 1. Denote the scaling dynamics: $\hat{\pi}^{sca} = \begin{bmatrix} \operatorname{diag}(\boldsymbol{\gamma}) & \mathbf{0} \\ \mathbf{0} & 1 \end{bmatrix}$ and its Lie group $H \subset \operatorname{Sim}(m)$, where $\operatorname{Sim}(m)$ is a similarity group. They satisfy the conditions in Proposition 1.

Proof. In the case of translation transformation $\hat{\pi}^{tra}$, for identity matrices, we have $I_m I_m = I_m I_m$. Also, we have $I_m \times v = v$ for $\forall v \in \mathbb{R}^m$. Therefore translation transformation $\hat{\pi}^{tra}$ satisfies the condition in Proposition 1. In the case of scaling transformation $\hat{\pi}^{sca}$, for diagonal matrices, we have $\operatorname{diag}(\gamma_1)\operatorname{diag}(\gamma_2) = \operatorname{diag}(\gamma_2)\operatorname{diag}(\gamma_1)$. Also, we have $\operatorname{diag}(\gamma_1) \times \mathbf{0} = \mathbf{0}$. Therefore scaling transformation $\hat{\pi}^{sca}$ satisfies the condition in Proposition 1.

A.5 Proof of Corollary 3

Corollary 4 (Equivariance of Second-Order Composed Transformations). The second-order composition of the planar rotation, translation, and scaling transformations defined in Corollaries 1–2 satisfies the commutativity conditions in Proposition 1. Specifically, for any $\hat{\pi}^{(1)}, \hat{\pi}^{(2)} \in \{\hat{\pi}^{rot}, \hat{\pi}^{tra}, \hat{\pi}^{sca}\}$, we have that $\hat{\pi}^{(1)}\hat{\pi}^{(2)}$ and its Lie group $H \subset \text{Aff}(m)$ satisfy the conditions in Proposition 1.

Proof. To show that $\hat{\pi}^{(1)}\hat{\pi}^{(2)}$ satisfies the commutativity conditions in Proposition 1, we need to

$$\hat{\pi}^{(1)}(g_1)\hat{\pi}^{(2)}(g_2)\hat{\pi}^{(1)}(h_1)\hat{\pi}^{(2)}(h_2) = \hat{\pi}^{(1)}(h_1)\hat{\pi}^{(2)}(h_2)\hat{\pi}^{(1)}(g_1)\hat{\pi}^{(2)}(g_2), \forall g_1, g_2, h_1, h_2 \in H.$$

Since $\hat{\pi}^{(1)}, \hat{\pi}^{(2)} \in \{\hat{\pi}^{rot}, \hat{\pi}^{tra}, \hat{\pi}^{sca}\}$ which already satisfy the commutativity conditions as shown in Corollaries 1-2, we have

$$\hat{\pi}^{(1)}(g_1)\hat{\pi}^{(1)}(h_1) = \hat{\pi}^{(1)}(h_1)\hat{\pi}^{(1)}(g_1), \quad \forall g_1, h_1 \in H$$

$$\hat{\pi}^{(2)}(g_2)\hat{\pi}^{(2)}(h_2) = \hat{\pi}^{(2)}(h_2)\hat{\pi}^{(2)}(g_2), \quad \forall g_2, h_2 \in H$$

Thus, the initial condition is reduced to showing that $\hat{\pi}^{(1)}$ and $\hat{\pi}^{(2)}$ can be commutative, i.e.,

$$\hat{\pi}^{(1)}(g)\hat{\pi}^{(2)}(h) = \hat{\pi}^{(2)}(h)\hat{\pi}^{(1)}(g), \quad \forall g, h \in H$$

Consider two transformations $\hat{\pi}^{(1)}, \hat{\pi}^{(2)} \in \{\hat{\pi}^{rot}, \hat{\pi}^{tra}, \hat{\pi}^{sca}\}$, their general affine transformation form is:

$$\hat{\pi}^{(k)} = \begin{bmatrix} A^{(k)} & \boldsymbol{b}^{(k)} \\ \boldsymbol{0} & 1 \end{bmatrix}, \quad \text{for } k = 1, 2,$$

$$\begin{array}{l} \text{where } A^{(k)} \in \mathbb{R}^{m \times m} \text{ and } \boldsymbol{b}^{(k)} \in \mathbb{R}^{m}. \text{ We have:} \\ \hat{\pi}^{(1)} \hat{\pi}^{(2)} = \begin{bmatrix} A^{(1)} A^{(2)} & A^{(1)} \boldsymbol{b}^{(2)} + \boldsymbol{b}^{(1)} \\ \boldsymbol{0} & 1 \end{bmatrix}, \quad \text{ and } \quad \hat{\pi}^{(2)} \hat{\pi}^{(1)} = \begin{bmatrix} A^{(2)} A^{(1)} & A^{(2)} \boldsymbol{b}^{(1)} + \boldsymbol{b}^{(2)} \\ \boldsymbol{0} & 1 \end{bmatrix}. \end{array}$$

According to Proposition 1, commutativity holds if:

$$A^{(1)}A^{(2)} = A^{(2)}A^{(1)}$$
 and $A^{(1)}\boldsymbol{b}^{(2)} + \boldsymbol{b}^{(1)} = A^{(2)}\boldsymbol{b}^{(1)} + \boldsymbol{b}^{(2)}$

We now verify these two conditions for all combinations:

- (i) **Linear Part:** $A^{(1)}A^{(2)} = A^{(2)}A^{(1)}$
 - If both are diagonal scaling matrices, this holds since diagonal matrices commute.
 - If both are planar rotations in the same subspace, they commute by the abelian property of SO(2).
 - If either matrix is I_m (as in translation), the product trivially commutes.
 - If one is scaling (diagonal) and the other is a planar rotation, they commute within the rotation subspace or when scaling is isotropic.
- (ii) Translation Part: $A^{(1)}b^{(2)} + b^{(1)} = A^{(2)}b^{(1)} + b^{(2)}$
 - If both transformations are translations, $A^{(1)} = A^{(2)} = I_m$, and the equality holds
 - If one is translation and the other is rotation or scaling, we have:

$$A^{(1)}\boldsymbol{b}^{(2)} = \boldsymbol{b}^{(2)}, \quad A^{(2)}\boldsymbol{b}^{(1)} = \boldsymbol{b}^{(1)},$$

since translation has $A^{(k)} = I_m$, satisfying the equality.

• If both are non-translation (rotation or scaling), $b^{(1)} = b^{(2)} = 0$, and the equality holds.

In all cases, the matrix product and translation terms satisfy the required commutation conditions. Therefore.

$$\hat{\pi}^{(1)}\hat{\pi}^{(2)} = \hat{\pi}^{(2)}\hat{\pi}^{(1)}$$
.

and the composed transformations satisfy the conditions of Proposition 1.

В Tasks, Data Generation, and Preprocessing

B.1 Interpolation and Extrapolation Tasks

We adopt a standard formulation consistent with prior work on continuous-time and irregularly sampled time series, such as Latent ODE, Contiformer, RNN- Δ_t , etc. The setup is as follows:

- (1) Interpolation. Given a time series with time points (t_0, \dots, t_N) , we condition on the subset of points from (t_0, \dots, t_N) with a data drop rate (30%, 60%, 90% in Experiments) and reconstruct the full set of points in the same time interval.
- (2) Extrapolation. We split the time series into two parts $(t_0, \dots, t_{N/2})$ and $(t_{N/2}, \dots, t_N)$. We input the first half of the time series and predict the second half. We apply the same random drop procedure only on the input half, and the model is tasked with predicting the entire future segment beyond the observed range.

B.2 Complex ODE systems

Spiral dataset. We generate 80 trajectories with 60 timesteps. The spiral system is a two-dimensional system with rotation and scaling symmetries, characterized by the infinitesimal generator v = $x_2\partial_1 - x_1\partial_2$ (i.e., $\begin{bmatrix} 0 & 1 \\ -1 & 0 \end{bmatrix}$ in matrix terms). It is governed by:

$$O_1 - x_1 O_2$$
 (i.e., $\begin{bmatrix} -1 & 0 \end{bmatrix}$ in matrix terms). It is governed by:

$$\begin{cases} \dot{x}_1 = -0.1x_1 - x_2, \\ \dot{x}_2 = x_1 - 0.1x_2, \end{cases}$$
 (17)

We also create more complex ODE systems with nonlinear symmetries.

Glycolytic Oscillator. We generate 100 trajectories, each with 200 timesteps. The two-dimensional Glycolytic Oscillator system [73] models a biochemical process governed by a pair of coupled ODEs with complex cubic nonlinear interactions. We adopt the same parameter settings as used in [37]. The governing equations are given by:

$$\begin{cases} \dot{x}_1 = 0.75 - 0.1x_1 - x_1x_2^2, \\ \dot{x}_2 = 0.1x_1 - x_2 + x_1x_2^2, \end{cases}$$
(18)

Lotka-Volterra System. We generate 100 trajectories, each with 200 timesteps. The two-dimensional Lotka-Volterra System is a classical model in population dynamics that describes the nonlinear interactions between predator and prey species. It is governed by the following coupled ODEs:

$$\begin{cases}
\dot{x}_1 = 0.1x - 0.02x_1x_2, \\
\dot{x}_2 = 0.01x_1x_2 - 0.3x_2,
\end{cases}$$
(19)

B.3 Power system datasets

Electricity consumption. We gather load consumption of Flores, Azores Islands in the year of 2008 [51]. The profile contains 366 days' load data with a sampling interval of 10min. We treat each day's data (144 points) as a trajectory and gather 100 trajectories.

Solar energy generation. We use a publicly available photovoltaic (PV) dataset [54] that records sequential solar power generation measurements. The data was collected in 2017 from a weather station located on the Gaithersburg, Maryland campus of the National Institute of Standards and Technology (NIST), with a sampling interval of 1 minute. We select data from four different locations and treat each day at each location as an individual trajectory, resulting in a total of 124 trajectories for a one-month period. To focus on periods with active solar generation, we remove nighttime measurements with zero output and extract 100 valid time steps per trajectory.

Event measurements. Following [74, 75], we simulate power system events using the commercialgrade Positive Sequence Load Flow (PSLF) software [76] developed by General Electric (GE). The simulations are based on the publicly available Illinois 200-node system [77]. Each simulation spans 4 seconds with a sampling interval of 33.33 milliseconds, capturing high-resolution system dynamics. We extract measurements from 100 selected nodes, treating each node's time series as a separate trajectory. This results in 100 trajectories, each containing 100 time steps. Each trajectory contains 10-dimensional data: voltage magnitude, voltage angle, current magnitude, current angle, frequency, rate of change of frequency, rotor speed, rotor angle, active power, and reactive power.

B.4 Weather system dataset

Air quality. We consider air quality data from the UCI repository [78], which contains the hourly responses of a gas multisensor device deployed on the field in an Italian city. Specifically, we use the C6H6 (GT) feature, which records the hourly averaged benzene concentration (in μ g/m³). We select the period from October 1, 2004 to December 13, 2004, containing 73 days of measurements without outliers. We treat each day's data (24 points) as a trajectory and gather 92 trajectories.

B.5 Biomedical system dataset

The signals correspond to electrocardiogram (ECG) shapes of heartbeats for the normal case and the cases affected by different arrhythmias and myocardial infarctions. We employ the ECG200 in [59]. The training data contains 100 trajectories, each with 97 timesteps.

C Introduction of Baseline Methods in Experiments

The following baseline methods are used. For interpolation, we have: (1) **EqSINDy** [37]. EqSINDy adds equivariance regularization to SINDy method to discover the symbolic equations for the ODE data. The equivariance relation is discovered through a GAN-based framework [40]. (2) EqGP [37]. Similar to EqSINDy, the equivariance relation is added to a Generic programming to discover symbolic ODE equations. (3) **RNN**- Δ_t [79]. The time difference between every two observations, i.e., Δ_t , is introduced to a classic RNN model. (4) **ODE-RNN** [18]. ODE-RNN can be directly utilized for dynamic learning in an encoder-only framework. (5) **Neural CDE** (**NCDE**) [17]. Neural CDE creates a continuous data path to control the evolution of the state's ODE flow. (6) ContiFormer [80]. ContiFormer is a Transformer-based with a continuous attention mechanism to extract feature flows at arbitrary times, (7) **Latent ODE** [18]. The model is illustrated in Section 2.3. For extrapolation, in addition to the above methods, we introduce the state-of-the-art Transformer-based methods for time-series forecasting: (8) **Informer** [81]. Informer is a transformer variant tailored for time-series forecasting, using a probabilistic sparse self-attention mechanism to reduce computation and improve efficiency. (9) Autoformer [82]. Autoformer enhances time-series prediction by introducing series decomposition and autocorrelation-based attention, enabling it to better model trend and seasonal patterns. As Informer and Autoformer can't process irregularly-sampled data, we conduct spline interpolation to pre-process input data for extrapolation tasks. For fair comparisons, we maintain roughly the same size of the hidden state, number of layers, and units among different methods. Architecture details and training time are reported in Appendix D and Appendix E.3, respectively.

D Model Architecture and Hyper-parameters

Computing infrastructure. All experiments were run in Python 3.12 on a Mac machine equipped with an Intel Core i5 processor (3.1 GHz) and 8 GB of RAM.

For fair comparisons, we maintain roughly the same size of the hidden state, number of layers, and units. In particular, we make the dimension of the latent space \mathcal{Z} , i.e., m, to be the same for Latent ODE and latent MoS. We also restrict them to having the same ODE-RNN encoder. The specific architectures and hyper-parameters are described as follows.

Encoder. Similar to Latent ODE [18], we employ an ODE-RNN as the encoder, as illustrated in Equation (4). In this ODE-RNN, we set the GRU module the same as the commonly used GRU baseline model, where the update gate, reset gate, and state transition module have two hidden layers with the hidden unit number to be m (specific values are shown in the following parts). The ODE function module also has two hidden layers with the hidden unit number to be m. The ODE solver used to solve the ODE-RNN is the fourth-order Runge-Kutta method ("rk4").

Decoder. The decoder is composed of the parameterized Lie group representation and the gating neural network. For each of the network, we still consider two hidden layers with the number of neuron to be m. Their output dimensions are directly related to m and K, which have been illustrated in the main section.

Multi-level MoS. In our decoder, we consider S=2 levels for multi-level MoS (see Section 3.3). Moreover, we set $L^1=2$ and $L^2=5$ to extract multi timescale equivariances.

Output layers. There are two hidden layers with the number of units to be m.

Activation function and learning rate. We utilize Tanh as the activation function, similar to Latent ODEs. We set the learning rate to be 0.001.

Restrictions on each of the Lie group actions. To enable smooth transitions, we enforce certain restrictions on the Lie group transition during Δt . Specifically, for rotational symmetry, we assume θ in R_{θ} to be within [-0.6, 0.6]. For translation symmetry, we assume the maximum norm of $v(\boldsymbol{z}(t), t)$ to be less than 0.001. For scaling symmetry, we assume $-1.5 \le \gamma(\boldsymbol{z}(t), t) \le 1.5$. These restrictions can be easily achieved by using Tanh activation. Further, to avoid scaling and translation dynamics leading to vanishing or exploding latent vectors, we rescale the norm of $\boldsymbol{z}(t_i)$ into (0.5, 1.5).

Gating mechanism. We encourage the exploration in the gating mechanism by assuming a warmup period where we don't restrict any sparsity to the gating values. After 10 epoch for the warmup, we select the top $K_0 \le K$ experts to build the mixture of latent flows.

Hyper-parameters We establish two important hyper-parameters for different datasets: the dimension of the latent space m and the number of experts K_0 for non-zero outputs. Specifically, they are shown in the following table.

Table 2: Hyper-parameter settings for different datasets.

System	Spiral	Glycolytic	Lotka	Load	Solar	Power event	Air quality	ECG
Latent dimension m	15	15	15	15	15	30	15	15
Non-zero gate numbers K_0	2	2	4	4	4	6	4	6

Table 3: Test Mean Squared Error (MSE) ($\times 10^{-2}$) for interpolation tasks under varying drop rates.

Data	Drop	EqSINDy	EqGP	RNN- Δ_t	ODE-RNN	NCDE	Contiformer	Latent ODE	Latent MoS
	90%	11.21	13.88	9.39	11.47	16.30	3.23	2.30	1.93
Spiral	60%	5.67	6.97	4.02	11.01	11.39	1.66	1.23	0.97
•	30%	2.12	2.13	2.05	10.97	8.03	1.32	1.14	0.74
	90%	14.45	23.09	14.28	14.08	31.90	4.66	11.24	0.33
Glycolytic	60%	6.38	10.58	7.76	13.54	22.82	2.89	2.68	0.21
	30%	2.74	4.26	2.34	13.27	17.44	0.43	1.64	0.18
	90%	13.45	10.98	11.22	3.75	38.13	2.21	2.63	0.53
Lotka	60%	7.88	4.77	6.26	3.34	28.21	0.92	0.22	0.30
	30%	2.42	1.61	2.43	3.26	20.55	0.91	0.09	0.06
	90%	18.98	16.79	8.53	3.51	14.88	6.61	2.76	2.30
Load	60%	8.45	7.74	3.13	2.37	18.25	4.50	0.97	1.10
	30%	5.21	4.37	1.37	2.23	20.78	4.45	0.89	0.90
	90%	15.89	13.79	40.21	5.69	32.07	11.96	4.01	3.10
Solar	60%	13.57	14.23	16.09	3.94	24.39	12.06	2.65	1.23
	30%	10.11	10.87	6.43	3.78	14.37	12.21	1.73	0.98
	90%	8.44	6.89	12.95	5.71	15.21	5.09	5.41	4.06
Power event	60%	6.58	4.53	8.82	5.22	14.52	4.34	4.17	3.65
	30%	3.28	3.75	4.34	5.13	12.02	3.40	4.01	3.14
	90%	15.89	18.70	17.38	4.76	26.70	7.53	4.36	3.30
Air quality	60%	15.23	15.99	12.18	3.27	14.61	8.12	3.16	2.24
	30%	10.98	14.03	6.23	2.88	8.78	6.73	2.30 1.23 1.14 11.24 2.68 1.64 2.63 0.22 0.09 2.76 0.97 0.89 4.01 2.65 1.73 5.41 4.17 4.01	1.53
	90%	13.41	10.09	10.42	6.37	13.56	5.02	2.87	1.15
ECG	60%	5.62	3.21	4.99	5.52	11.03	3.17	1.42	0.56
	30%	3.08	1.05	2.28	5.41	9.92	3.07	1.35	0.34

E Supplementary Experimental Results

E.1 Table of Interpolation Results

We present the tabular results for Fig. 3 as follows. Contiformer, Latent ODE, and Latent MoS can learn the continuous latent ODE in the decoding process, thus achieving the best performances. Among them, Latent MoS leverages geometric priors to structure the latent trajectories. Across all datasets, Latent MoS achieves relative improvements ranging from 15% to 97%.

E.2 Predicted Curve Visualization

We visualize the predicted trajectories of three complex ODE systems, including the Spiral system, the Glycolytic Oscillator, and the Lotka-Volterra system, under low-resolution data conditions with a drop rate of 90%. The ground truth trajectories are shown as black curves, the observed low-resolution data points are plotted as blue dots, and the predicted trajectories from both the Latent ODE model and our proposed Latent MoS model are illustrated as orange dashed curves. As shown in Fig. 6, the Latent MoS model consistently provides more accurate reconstructions of the underlying dynamics, which we attribute to its enhanced capability to preserve hidden symmetries in the data.

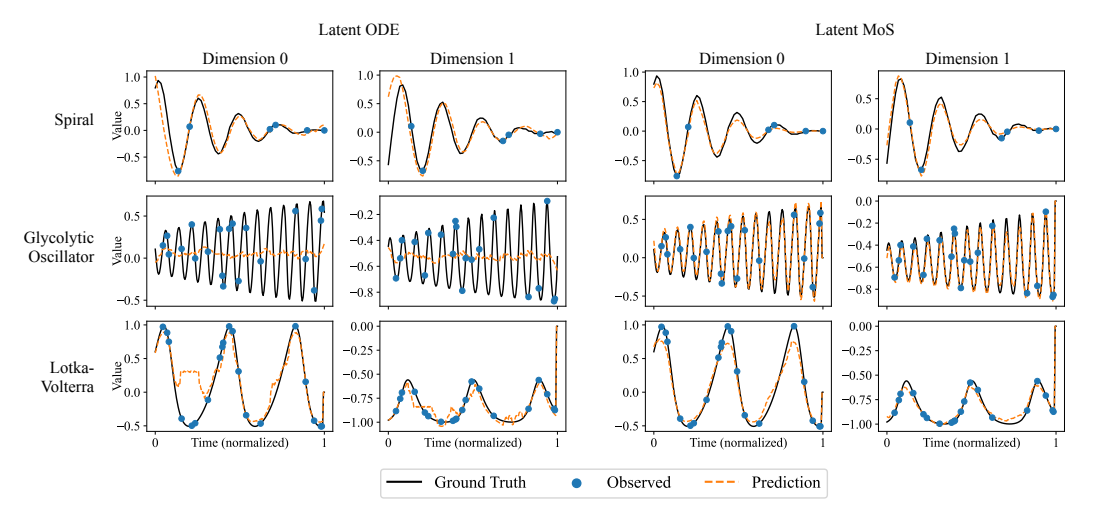


Figure 6: Comparison of ground truth trajectory and predicted trajectory for three complex ODE systems (Spiral, Glycolytic Oscillator, and Lotka-Volterra) under low-resolution data with a 90% drop rate.

E.3 Training Time

We report the training time for different models in the following table. The results show that our methods can achieve relatively moderate training time, comparable to Latent ODE and ODE-RNN. We eliminate the results EqSINDy and EqGP methods because they require separate symmetry discovery and symbolic regression processes.

Table 4: Training time (minutes) for different systems and models.

racio il Training timo (minutos) for different systems and medels.											
RNN- Δ_t	ODE-RNN	NCDE	Contiformer	Informer	Autoformer	Latent ODE	Latent MoS				
4.9	6.5	46.4	111.2	70.7	58.5	7.3	8.4				
7.7	10.4	81.2	162.5	121.9	91.7	12.2	15.5				
9.4	10.2	74.5	193.3	125.9	90.3	12.6	15.4				
7.5	10.1	80.4	168.8	120.6	98.5	12.0	13.4				
11.4	13.4	83.6	204.1	150.6	112.5	15.7	18.1				
15	19.4	118.8	317.4	211.6	165.6	21.2	25.4				
6.0	6.7	53.0	116.9	85.8	63.2	8.4	10.0				
6.8	9.2	59.7	153.3	103.9	76.4	10.4	13.3				
	RNN- Δ_t 4.9 7.7 9.4 7.5 11.4 15 6.0	$\begin{array}{ccc} \text{RNN-}\Delta_t & \text{ODE-RNN} \\ 4.9 & 6.5 \\ 7.7 & 10.4 \\ 9.4 & 10.2 \\ 7.5 & 10.1 \\ 11.4 & 13.4 \\ 15 & 19.4 \\ 6.0 & 6.7 \\ \end{array}$	$\begin{array}{c cccc} RNN-\Delta_t & ODE-RNN & NCDE \\ \hline 4.9 & 6.5 & 46.4 \\ 7.7 & 10.4 & 81.2 \\ 9.4 & 10.2 & 74.5 \\ 7.5 & 10.1 & 80.4 \\ 11.4 & 13.4 & 83.6 \\ 15 & 19.4 & 118.8 \\ 6.0 & 6.7 & 53.0 \\ \hline \end{array}$	$\begin{array}{c ccccccccccccccccccccccccccccccccccc$	$ \begin{array}{c ccccccccccccccccccccccccccccccccccc$	$ \begin{array}{c ccccccccccccccccccccccccccccccccccc$	$ \begin{array}{c ccccccccccccccccccccccccccccccccccc$				